BNL-NUREG -28961
INFORMAL REPORT
LIMITED DISTRIBUTION

A STUDY OF THE FEASIBILITY OF MICROWAVE DIELECTRIC HEATING FOR LMFBR TRANSITION PHASE ACCIDENT SEQUENCE BOILING STUDIES

By

H. Makowitz and T. Ginsberg

DATE PUBLISHED - JANUARY 1981

EXPERIMENTAL MODELING GROUP

DEPARTMENT OF NUCLEAR ENERGY BROOKHAVEN NATIONAL LABORATORY
UPTON, NEW YORK 11973

NRC Research and Technical Assistance Report

Prepared for the U.S. Nuclear Regulatory Commission
Office of Nuclear Regulatory Research
Contract No. DE-AC02-76CH00016

NOTICE

BNL-NUREG-28961
INFORMAL REPORT
LIMITED DISTRIBUTION

A STUDY OF THE FEASIBILITY OF MICROWAVE DIELECTRIC HEATING FOR LMFBR TRANSITION PHASE ACCIDENT SEQUENCE BOILING STUDIES

By

H. Makowitz and T. Ginsberg

Experimental Modeling Group
Department of Nuclear Energy
Brookhaven National Laboratory
Upton, New York 11973

January 1981

Prepared for the U.S. Nuclear Regulatory Commission
Office of Nuclear Reactor Research
FIN No. A-3024

ABSTRACT

A study is reported on the feasibility of the use of microwave dielectric heating to simulate the nuclear heat source in LMFBR "transition phase" accident sequence volume-boiling simulation experiments. The adequacy of microwave heating is judged based upon the criterion of heating uniformity per unit liquid volume and upon the ability to analytically characterize the liquid power density distribution.

Two aspects of liquid power density uniformity are addressed. First, the effect of liquid geometry on power density is studied in order to determine whether millimeter-size droplets can be heated as efficiently as centimeter-scale masses which are exposed to the same source of radiation. Both analyses and experiments were performed in this portion of the study. Second, the spatial distribution of power density across liquid slabs is studied, in order to determine whether wave interference effects, which lead to severe power density gradients, can be minimized by choice of suitable dielectric liquids. The above analyses were carried out for a variety of wavelengths within the microwave radiation band, for several dielectric liquids and for a range of temperature.

Microwave oven irradiation of water as the test fluid was considered as one alternative. The results of the analyses lead to the conclusion that water droplets in the millimeter-diameter size range absorb 1-2 orders of magnitude less energy per unit liquid volume than centimeter-scale droplets exposed to the same source of radiation. Laboratory microwave oven experiments, albeit in different geometry, support this conclusion. In addition, the analyses of the slab irradiation problem suggest that standing waves are generated within slabs due to wave interference effects. These standing waves, together with attenuation due to dielectric losses, are responsible for power density gradients across slabs. These gradients are expected to exist in a microwave oven environment and cannot be predicted with state-of-the-art analytical methods. The existence of power density gradients is supported by experiments performed in the laboratory, and by previous work reported in the literature.

Alternate test fluids were considered. It was concluded that a fluid, cyclohexane-ethanol, can be found which would ensure efficient heating of a dispersed droplet regime. A microwave oven radiation environment however,

provides neither heating uniformity nor the ability to predict the power density distribution. The judgement is made, therefore, that it is not appropriate to use a microwave oven for the boiling simulation studies.

The concept of using a microwave waveguide to irradiate the boiling dielectric liquid was investigated. The waveguide would be operated in a single mode, and would be driven by two sources of slightly different frequency. If impedance matching techniques can be successfully used to eliminate the internally reflected waves within the boiling dielectric liquid, and if the dielectric properties of the two-phase mixture can be represented analytically, then the power density distribution can be predicted. In addition, the microwave energy flux distribution can be measured along the axis of the waveguide. A microwave wavelength of 300 mm would minimize power density gradients due to dielectric loss attenuation.

It is concluded that the use of microwave heating, while not straightforward, is feasible for simulation of the nuclear heat source in transition phase boiling studies. A waveguide microwave radiation field, with a cyclohexane-ethanol test fluid, together will satisfy two of the major requirements of the proposed boiling experiments: predictability of the power density distribution, and efficient heating of the liquid phase in a dispersed droplet flow regime.

TABLE OF CONTENTS

Table of Contents (Continued)

Table of Contents (Continued)

Table of Contents (Continued)

LIST OF FIGURES

List of Figures (Continued)

List of Figures (Continued)

LIST OF TABLES

NOMENCLATURE

a	droplet radius
A	frontal area of droplet
A'	optical density
$A_{s,H}$	surface area of liquid sample of height H
$A_{s,REF}$	surface area of reference sample
$\vec{B}$	magnetic induction vector
c_g	heat capacity of glass
c_l	heat capacity of liquid
C_{ABS}	absorption cross section
C_{EXT}	extinction cross section
C_{SCAT}	scattering cross section
$\vec{D}$	dielectric displacement vector
$\vec{E}$	electric field intensity vector
E_o	incident electric field intensity
f	frequency
f_c	cutoff frequency
H	height of liquid in test tube
$\vec{H}$	magnetic field intensity vector
j	$\sqrt{-1}$ unit complex number
k	index of absorption
k^*	complex relative permittivity
k'	real part of relative permittivity
k''	imaginary part of relative permittivity
k_m^*	complex relative permittivity
k_m'	real part of relative permeability

k_m''	imaginary part of relative permeability
ℓ	slab thickness
m^*	complex index of refraction
m_g	mass of glass
m_ℓ	mass of liquid
n	real part of index of refraction
n'	imaginary part of index of refraction
P	energy absorption rate
Q_{ABS}	particle energy absorption efficiency
Q_H'''	power density of liquid sample of height H
Q_{REF}'''	power density of reference container liquid
Q'''	local rate of energy production per unit total volume
Q_v'''	local rate of energy production per unit volume vapor
Q_ℓ'''	local rate of energy production per unit volume liquid
r_i	reflection coefficient
t	time
t_i	transmission coefficient
$\tan \delta$	loss tangent
T	temperature
V	droplet or particle volume
V_H	volume of liquid sample of height H
V_{REF}	volume of reference sample
x	slab thickness coordinate
Z	impedance

Greek Symbols

α	attenuation factor

α_v	void fraction (volume fraction vapor)
β	phase factor
β'	attenuation coefficient
γ^*	complex propogation factor
ε^*	complex electrical permittivity
ε'	real part of electrical permittivity
ε''	imaginary part of electrical permittivity
ε_o	permittivity of free space
λ	free space wavelength
λ_m	wavelength in dielectric material
μ^*	complex magnetic permeability
μ'	real part of magnetic permeability
μ''	complex part of magnetic permeability
μ_o	magnetic permeability of free space
ρ_g	density of glass
ρ_l	density of liquid
Φ_{INC}	incident electromagnetic energy flux
ψ	dimensionless power density

I. INTRODUCTION

1.1 Objectives

Modeling of hypothetical core disruptive accidents (HCDA's) is an important feature of liquid-metal fast breeder reactor (LMFBR) safety analysis. Both in-pile and out-of-pile simulation experiments have been performed in support of the analytical efforts. Simulation of the nuclear heat source has been accomplished, where necessary, for the most part by electrical resistive heating. Recently, however, consideration has been given to simulation of aspects of the "transition phase" (Greene, 1980) of the loss-of-flow (LOF) accident. This accident phase may be characterized by temporary entrapment of boiling pools of molten fuel and steel within the original core boundaries. Experiments to investigate the multiphase flow and heat transfer characteristics of such systems have been performed (Farahat, 1976; Koontz, 1977) and are planned in which simulant fluids are volume-heated by microwave electromagnetic radiation. The investigation reported here was performed to evaluate the usefulness of microwave dielectric heating as a simulator of the nuclear heat source in transition phase boiling pool simulation experiments.

Figure 1.1 is a schematic representation of an LMFBR in a disrupted configuration. Part of the reactor core is molten, and some fuel assemblies contain molten, boiling mixtures of fuel and steel. Figure 1.2 shows a fuel assembly in a molten, boiling configuration. Laboratory simulations of the boiling dynamics within such a system require development of a heat source which adequately simulates that of nuclear heating.

The nuclear heat source is distributed volumetrically within the fuel. If the fuel is fission-heated, then the spatial distribution of the heating rate is determined by the neutron flux distribution. If the fission rate is negligible, then the heating rate is determined by fission product decay, the magnitude of which depends on the time elapsed since reactor shutdown and on the previous operating history of the fuel.

In a two-phase molten fuel mixture of liquid and vapor, the local volumetric rate of energy production (or the power density) is given by

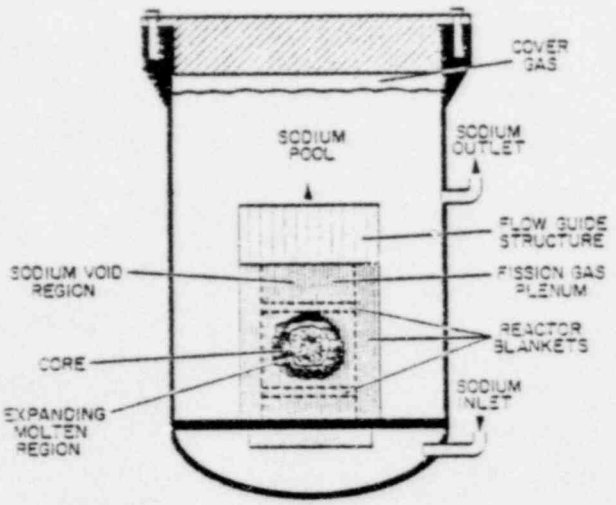

Figure 1.1 Schematic of Disrupted LMFBR Core.

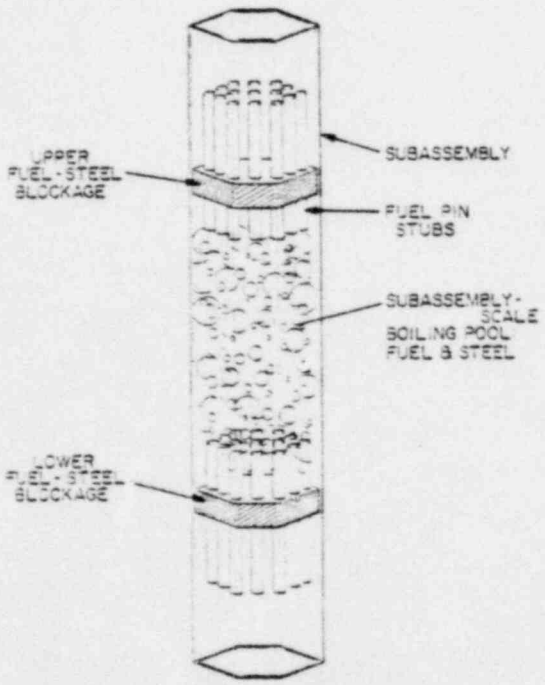

Figure 1.2 Representative Disrupted Fuel Assembly.

$$Q''' = = \alpha_v Q'''_v + (1 - \alpha_v) Q'''_\ell \qquad (1.1)$$

where Q'''_v and Q'''_L are the power densitites of the pure vapor and pure liquid, respectively. The vapor contribution, in general, can be neglected, and the rate of energy generation is proportional to the local volume fraction of liquid.

The purpose of the experimental simulations of interest to transition phase studies is to provide data for development of models to characterize the spatial distribution of molten liquid and voids in boiling pools of fuel and steel. Simulations of prototypic decay heating power densities in pools of fuel assembly scale (100 mm laterally and 1-2m axially) are of interest. It is reasonable under these conditions to assume that the energy generation rate per unit volume of molten fluid is independent of position. The nuclear heat source simulation, therefore, should also have this characteristic. This may be difficult to achieve in practice, as will be shown later in this report. As a minimum requirement, the analytical model development demands that the spatial distribution of heating rate be either calculable or measurable (Ginsberg, 1979).

Low-frequency (60 Hz) electrical resistive heating has been employed in simulation studies of volume-heated boiling systems (Gabor, 1976; Ginsberg, 1979; Greene, 1979). Electrical heating, which requires liquid continuity between electrodes, has been used to study the boiling and heat transfer characteristics of volume-heated systems at relatively low power densities (up to 2% of steady state LMFBR power density). At such low power conditions the flow structure is either bubbly or churn-turbulent (Ginsberg, 1979) and liquid continuity is maintained between electrodes. At higher power densities, however, the vapor generated would likely lead to liquid breakup into droplets. When this occurs, liquid continuity between electrodes cannot be maintained and energy deposition in the droplets would not be possible. Under these conditions electrical heating becomes inappropriate and an alternate form of heating becomes necessary.

Microwave heating is potentially useful in the context of simulation of

nuclear heating at elevated power densities. This is based upon the expectation that "reasonably uniform" volumetric heating of a fuel simulant liquid can be achieved with a source of electromagnetic microwave energy remote from the fluid being heated. Thus, the need for liquid continuity would be eliminated, and droplets would be heated under these conditions.

The microwave heating principle has been employed (Farahat,1976; Koontz, 1977) in experimental simulations involving boiling of volume-heated liquid systems. In addition, a preliminary evaluation of microwave heating, as applied to simulation of fuel meltdown phenomena, has been published (Gabor, 1975). In the prior work, however, the adequacy of microwave heating as a simulation of nuclear heating was not addressed as it pertains to two-phase, vapor-liquid systems. The degree of uniformity and predictability of heating rates achievable using microwave heating of boiling systems were not defined. It is felt that resolution of these issues is fundamental to the use of microwave heating in the present context.

The present work is motivated by the need to simulate the volume-heated boiling flow processes which characterize molten mixtures of fuel and steel in subassembly-scale configurations, using microwave dielectric heating as a nuclear heat source simulator. The objectives of the present work are:

(i) to evaluate the microwave heating technique as applied to laboratory simulations of the boiling process to be carried out using appropriate simulants of liquid fuel.

(ii) to design an experimental system using microwave energy deposition in which to study the boiling multiphase flow processes in volumetrically-heated boiling fluids.

Sections 1.2 and 1.3 of this chapter present a review of the literature relevant to microwave heating of dielectric fluids in the present context. The scope of the remainder of the report is presented in Section 1.4.

1.2 Previous Work: Accident Simulation Studies.

1.2.1 ANL Feasibility Study (Gabor, 1975).

This study was performed to evaluate the applicability of microwave (and

induction) heating to laboratory simulations of selected phases of core meltdown accidents in LMFBR's. The work was directed primarily towards simulation of the flow and heat transfer processes which would occur during the fuel meltdown stage of HCDA's. The simulation considered was a complex one. Fuel, steel and sodium simulants were desired which, together with a volumetric microwave heat source in the fuel, would simulate the processes involved in meltdown, relocation and resolidification of the fuel and steel. Fuel and steel boiling processes were not considered. This simulation would require a combination of heat-generating and non-generating materials. The fuel simulant would be required to generate heat volumetrically at equal rates, in coexisting liquid and solid phases. The authors found that dielectric properties of potential fuel simulants were significantly different for solid and liquid phases. They concluded, therefore, that microwave heating could not supply the uniform heating rate required within the fuel simulants. Other difficulties were encountered with steel and sodium simulants. It was concluded that the laboratory simulation of the integral set of phenomena using microwave heating to simulate the nuclear heat source is impracticable.

The uniformity of microwave heating of single-phase liquid samples under microwave oven irradiation was studied empirically. Water samples were irradiated in a Litton microwave oven (600 W, 2450 MHz). The temperature rise of samples at different locations within the oven, and at different locations within the same sample, were measured after fixed irradiation times. The results of these calorimetric measurements are summarized below:

(i) The total power delivered to a single sample in a microwave oven depends on the mass of the sample. The power delivered to a 55 g water load was 352 watts, compared with 615 watts to a 1000 g load. This reduction in power "coupling" efficiency is a characteristic feature of all microwave ovens.

(ii) The power delivered to a fixed load mass depends on the sample position within the oven. A variation of 8% in delivered power to the sample was measured using 100 mℓ water samples.

(iii) A number of tests were performed to assess the spatial variation of heating rate within samples under irradiation. These tests were

carried out with both water and glycerol in cylindrical geometry (glass heaters) with various aspect ratios. The results were interpreted to indicate that the heating rates are reasonably uniform within any one sample volume.

Analysis of the spatial variation of power density within an object subjected to microwave radiation was performed assuming exponential attenuation of microwave "rays" incident upon the object. Planar and isotropic radiation incident on slabs, and isotropic incidence on spheres were evaluated in this manner. The governing parameter in this calculation is the optical density, defined by

$$A' = 2\,\beta'\,Z \qquad \text{for a slab}$$

or

$$A' = 2\,\beta'\,R \qquad \text{for a sphere}$$

where β' is the "attenuation coefficient" (Von Hippel, 1954).

As a result of their analysis the authors concluded that with optical densities in the range 0.3 - 0.6, power density variations would be approximately $\pm$ 10% across the object. For water at 373 K, this corresponds to Z or R in the range 30 - 60 mm.

The above analysis ignores the possibility of wave interference effects within the object under irradiation. Such effects may lead to much more severe heating variations than predicted using the ray attenuation approach.

1.2.2 Purdue Microwave Boiling Studies (Koontz, 1977)

Experiments were performed using microwave heating to study the boiling characteristics of volume-heated liquids. The tests were carried out to simulate, and to provide insight into, the boiling flow mechanisms of fuel-steel mixtures characteristic of LMFBR core disruptive accident conditions.

The tests were carried out in a 5 kW, 2450 MHz microwave oven. The cavity was a cube, 0.762 m (30 inches) on a side. Test vessels containing first water, and then mixtures of hexane and water, were used to study single and multi-component volume-boiling characteristics.

The efficiency of coupling of the microwave power to the water load was measured experimentally under boiling flow conditions. The efficiency for water

loads greater than 1000 mℓ was constant at 73%, and dropped off monotonically with volume below 1000 mℓ. At 200 mℓ, the efficiency was approximately 42%.

The liquid power density, required to characterize the boiling flow processes, was assumed independent of position within the liquid container under boiling conditions. Assuming constant efficiency, an average power density was then taken to be inversely proportional to the liquid volume. No attempt was made to characterize the spatial distribution of power density.

The boiling flow regimes encountered in this work were the bubbly and churn-turbulent regimes. A dispersed droplet regime was not observed. The vapor volume fraction in these experiments varied from zero to 0.9. This range of void fraction coexisted within the test container. Methods do not exist to enable one to determine the power density distribution under such conditions. The distribution of heating intensity within the boiling mixtures, therefore, is unknown. Hence, a uniform liquid power density was assumed.

1.2.3 ANL Microwave Boiling Experiments (Farahat, 1976)

Steady-state and transient boiling experiments were carried out using microwave heating. Steady-state boiling was observed in a 600 W oven, while transient measurements were made in a 2 kW oven. Both used 2450 MHz sources.

Water was used as the boiling fluid. It was observed, however, that the use of pure water in glass containers did not provide a bulk boiling environment. Plastic particulate, therefore, was added to provide bulk nucleation sites in order to promote volume-distributed boiling.

The power coupling efficiency was determined by calibration under non-boiling conditions. The uniformity of liquid power density within the boiling fluid system was not addressed.

Steady-state boiling was observed in glass containers ranging from 8 to 120 mm in diameter. Liquid sample volumes ranged from 9 to 500 mℓ. Under most of the boiling conditions a stratified boiling flow field was observed. At the bottom of the container was a region largely devoid of bubbles. Over this region, however, a high void fraction "foam" flow regime was observed. The average void fractions were greater than 0.9 for most of the experimental conditions.

The power density distributions under the above conditions are not known. In addition, the necessity for addition of bulk nucleation sites to promote volume-boiling conditions is at odds with the work of Koontz (1976) in which such additives were apparently not necessary.

1.3 Previous Work - Electromagnetic Wave Interactions with Matter.

The interaction of (non-ionizing) electromagnetic (E-M) radiation with matter has been widely studied. Most of this work has been carried out with relatively simple geometries in well-characterized radiation environments, e.g., plane polarized waves interacting with spheres, cylinders or slabs. Mathematical treatment of such interactions may be accomplished. For such cases, therefore, power density distributions in dielectrics exposed to microwave radiation can be adequately characterized. On the other hand, studies of interactions of media with complex irradiation environments such as in resonant microwave cavities (e.g., ovens) were less numerous. Mathematical characterization of power density distributions in microwave cavities is not well-developed, and relatively few experimental studies have been reported.

For the purposes of the present work, the literature on electromagnetic wave interaction with matter may be categorized in two parts:

(i) Work directed towards scattering and absorption of E-M waves from discrete objects such as spheres, cylinders, ellipsoids, etc. Computation and measurement of scattering, absorption and extinction cross-sections are the focal points of this literature. The spatial distribution of field strength within the objects are generally not of prime importance.

(ii) Research directed towards characterization of the field strength and other related parameters within the object under radiation.

Analytical approaches to both problem categories derive from solution of Maxwell's equations. They do, however, appear rather distinctly in the literature. Since both areas are of concern in the present work, the literature is reviewed separately below.

1.3.1 Electromagnetic Scattering and Absorption Theory.

The classical theory of light scattering from objects of various geometries is well established (Mie, 1908; Van de Hulst, 1957; Kerker, 1969). Given the dielectric properties of a scattering sphere, for example, one can compute the energy removed from an incident field of microwave energy by scattering and by absorption in the sphere. Computer codes based upon the theory are available which enable one to compute the scattering and absorption cross-sections as functions of object geometry, dielectric properties and incident radiation wave-length. The theory has been applied to homogeneous material objects and also to objects with a layered material structure. The theory developed applies to plane wave irradiation of the objects.

A typical result for spherical geometry, taken from Schwan (1968), is presented in Figure 1.3. The absorption cross-section shown in Figure 1.3 is defined such that the power absorbed by the sphere is

$$P = \Phi_{INC} Q_{ABS} A \qquad (1.2)$$

The absorption cross-section is presented as a function of dimensionless radius. The material properties are close to that of water. This result suggests that the power absorbed by spheres is a strong function of particle size.

In the present context, we are interested in a heat source which would heat a two-phase, liquid-vapor boiling mixture uniformly, independent of liquid geometry. Figure 1.3 suggests that if droplets are present in the boiling flow field then it may not be possible to uniformly heat them with microwave radiation if water is used as the dielectric liquid.

The scattering theory will not be reviewed here. A brief discussion of the methods is, however, presented in Section 2.2 and in more detail in Appendix A.

1.3.2 Electric Field and Power Density Distributions in Dielectrics.

A. "Simple" Source Environments.

Solutions to Maxwell's equations for dielectrics of various geometries

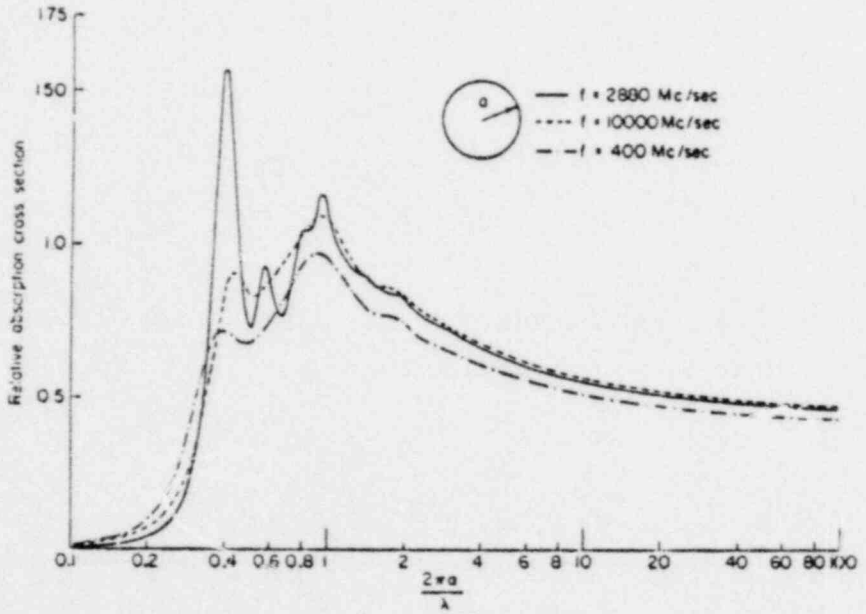

Figure 1.3 Relative Absorption Cross Section of a Sphere of Tissue-like Dielectric Properties at Three Different Frequencies, (Schwan, 1968). (BNL Neg. No. 12-1242-80)

exposed to E-M fields of a large spectrum of frequencies have been reported. Simple radiation sources, i.e., plane or linearly polarized incident fields, were generally assumed. Much of this work has been carried out in applications of E-M radiation for medical therapy and for evaluation of the adverse response of animal organisms to E-M fields.

Samples of animal body tissue, and also simulated body tissue, in slab, cylindrical and spherical geometries have been studied both analytically and experimentally (Johnson, 1972; Ho, 1971; Lin, 1973; Guy, 1971a). Multi-layered samples have also been studied (Guy, 1971b; Shapiro, 1971).

Calculation results for spherical geometry are shown in Figure 1.4. Predictions of power density distributions in spheres which simulate human and monkey brain tissue (both similar to water - in dielectric properties) are presented for two microwave frequencies. The results display rather severe power density gradients. The magnitude and shape of the distribution depend on frequency and sphere radius. In the case of the 140 mm spheres, the lower frequency (915 MHz) waves are focused towards the center of the sphere. At higher frequency (2450 MHz) preferential skin heating is observed.

The calculational methods used to generate the above results have been verified experimentally. Models of brain tissue (called "phantom" tissue) have been irradiated by plane waves for a given exposure time. The models were then split and infrared thermograms of the exposed samples were recorded. The local temperature rise is then proportional to the power density. Typical results are presented in Figure 1.5. Agreement with the analytical results are, in general, quite good.

Experimental and calculational results have also been obtained for slab and cylindrical geometry. Severe power density gradients are observed here also. Good agreement for slab geometries between plane wave theory and experiment has been demonstrated (Guy, 1971).

The results cited above suggest that:

(i) available methods can be used to predict the power density distributions in homogeneous or stratified objects of "regular" geometry, which are exposed to uniform incident plane wave sources of radiation,

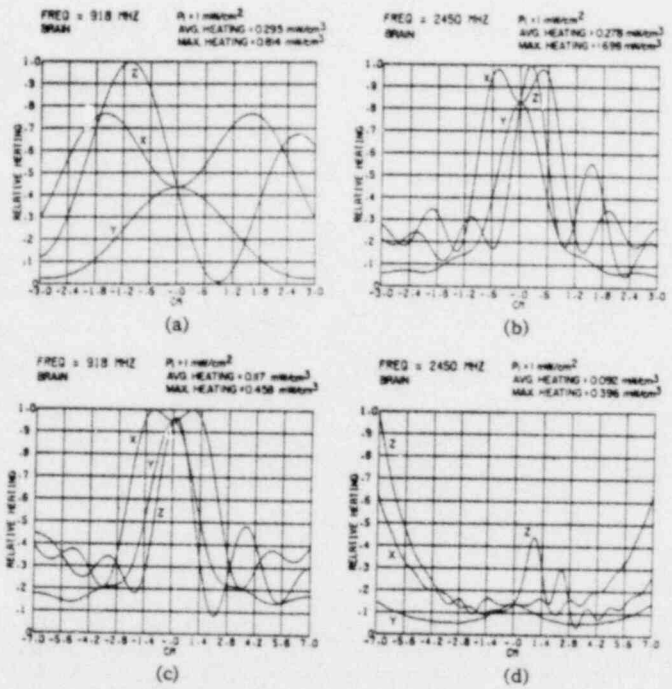

Theoretical absorbed power density patterns along the x, y, and z axes models of brain tissue exposed to a plane wave source. (Incident power density 1 mW/cm², propagation along the z axis, and electrical field polarized along the x axis with origin at center of sphere.)

Figure 1.4 Theoretical Absorbed Power Density Patterns (Johnson, 1972). (BNL Neg. No. 12-1240-80)

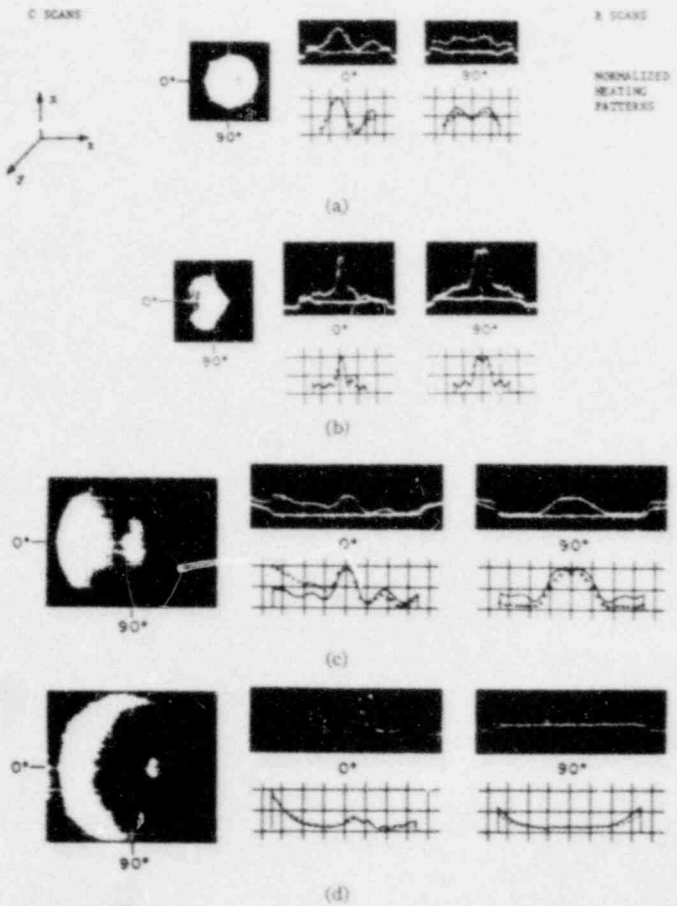

Thermograms of phantom brain tissue. Scale: *C* scans, 1 div = 2 cm; *B* scans, 1 horizontal div = 2 cm, 1 vertical div = 2.5°C; and normalized patterns, 1 horizontal div = 2 cm. (Propagation in *z* direction with *E* field polarized along *x* axis of indicated coordinates.) (a) 6-cm diam, 918 MHz. (b) 6-cm diam, 2450 MHz. (c) 14-cm diam, 918 MHz. (d) 14-cm diam, 2450 MHz. ———, plane wave theory; · · · · ·, experimental plane wave; ▲▲▲▲▲, experimental aperture source.

Figure 1.5 Thermograms of Phantom Brain Tissue (Johnson, 1972). (BNL Neg. No. 12-1241-80)

(ii) strong power density gradients have been observed in spherical, cylindrical and slab geometries, irradiated in microwave radiation fields with plane wave incidence.

B. "Complex" Source Environments.

The literature on the response of dielectrics exposed to complex radiation fields of resonant microwave cavities such as microwave ovens is extremely limited. A microwave power source is used to excite a closed metallic cavity into numerous electromagnetic modes of oscillation. The specific modes, and number of modes, are governed by the geometry of the cavity, the geometry and dielectric properties of the object under irradiation within the cavity and the source frequency (James, et al, 1968). In such a cavity, a sample is exposed to a radiation field which is composed of a superposition of the individual modes. It has been suggested (Crapuchettes, 1966) that the uniformity of heating in microwave ovens depends on the number of modes of excitation induced by the source. Various techniques have been proposed to enhance heating uniformity within irradiated samples. Mathematical methods, however, to enable one to compute the power density variation within samples placed in a microwave cavity are still in the developmental stage.

Only one rigorous mathematical treatment has been found in which the field within a sample irradiated in a microwave oven was analyzed (Watanabe, et al, 1978). The power density distribution in a water sample was computed and compared with experimental measurements. One sample geometry was considered, and only limited numerical results are presented. The analytical and experimental results for the power density compare favorably, both qualitatively and quantitatively. The power density distribution is not uniform, with variations of a factor of 3-4 observed across the sample.

Guy, et al, (1975) have presented results of power density measurements made on spherical and ellipsoidal samples irradiated in microwave ovens. Both 915 and 2450 MHz ovens were used in the experiments. Techniques similar to those employed in earlier tests (Guy, 1971) were employed. Infra-red thermography was used to measure temperature distributions in "phantoms" of human muscle tissue, after a fixed irradiation time. Results for 60 mm and 140 mm spheres are presented in Figure 1.6. These results indicate that highly non-uniform power density distributions are to be expected in spheres irradiated in

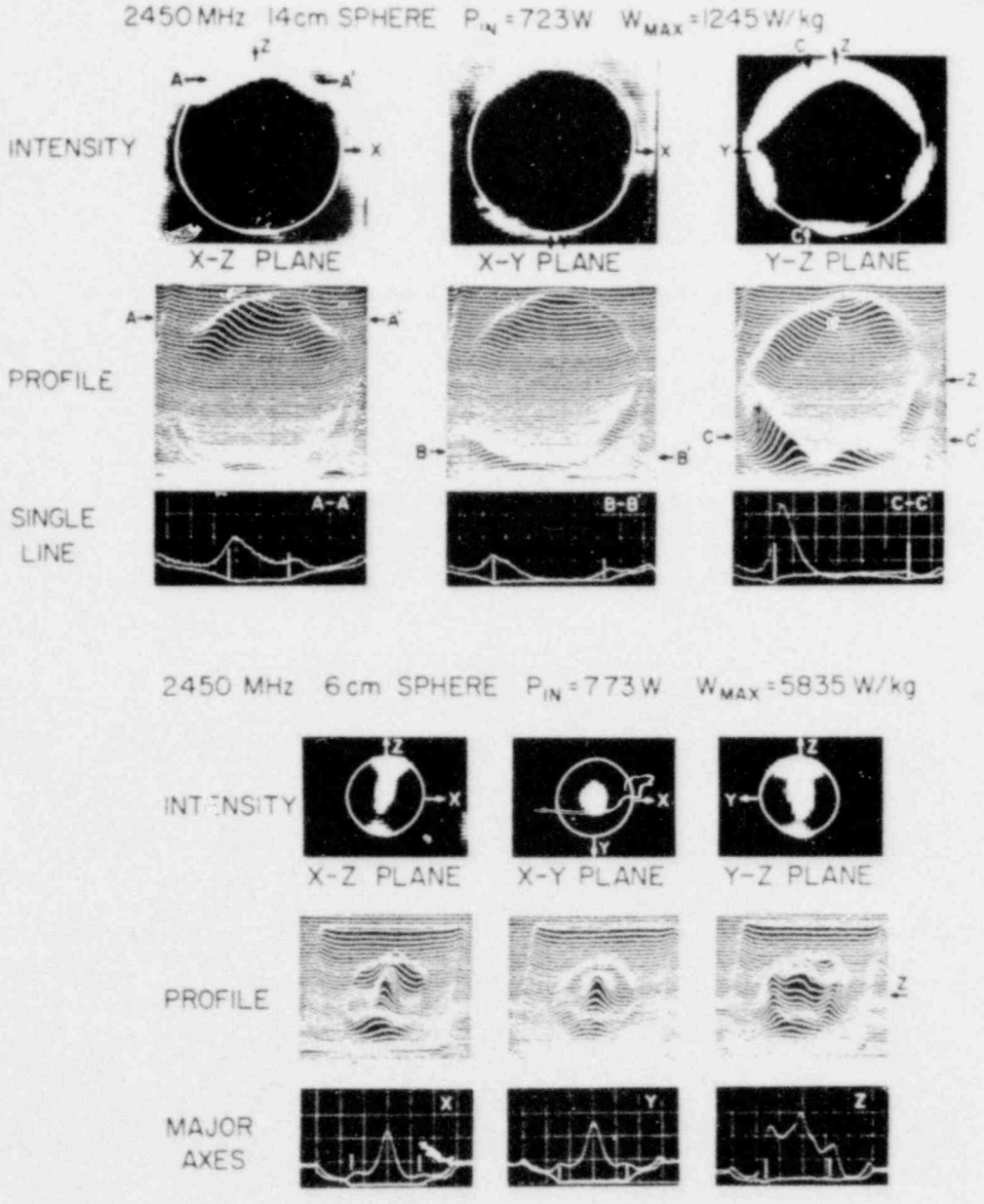

Thermograms illustrating power absorption patterns for 14 cm diameter sphere exposed in 2450 MHz and 918 MHz microwave ovens. Scale: horizontal - 1 div = 2 cm; vertical - 1 div = 3.33°C; vertical lines on single line scans indicate boundaries of object.

Figure 1.6 Thermograms Illustrating Power Absorption Patterns for 14 cm Diameter Spheres Exposed in 2450 and 918 MHz Microwave Ovens (Guy 1975). (BNL Neg. No. 12-1243-80)

microwave oven fields. Similar results could be expected for water, whose dielectric properties are similar to those of the "phantoms" studied by Guy. Similar non-uniform heating patterns were observed in ellipsoidal objects placed in the same ovens.

Ohlsson and Risman (1978) have performed experiments similar to those of Guy, et al, using spheres and cylinders. Strong power density gradients were observed for both geometries and for both 915 and 2450 MHz frequency irradiation fields.

Simple exponential attenuation models for the power density in cylindrical and slab geometries were employed by Nykuist (1977), Nykuist and Decareau (1976) and Ohlsson and Bengtsson (1971) to explain temperature profiles measured in various foods which were exposed in microwave ovens.

In the cylindrical geometry studies (using meat roasts) of Nykuist and Decareau, the temperature profiles did not indicate significant radial power density peaking. It was shown computationally, however, that the model predicts some peaking, preferentially for 915 MHz irradiation and for smaller diameter cylinders. The temperature profiles measured by Ohlsson and Bengtsson for slab geometries (in 30 mm thick slabs of beef or simulated beef) were also reaonably well characterized using exponential power observation through the material, irradiated in a 2450 MHz microwave oven. These experiments were carried out with the materials passing through the oven on a conveyor system (the oven was 1.5 m long).

1.4 Scope of Present Work.

The objective of the work described in this report is to evaluate the potential use of microwave dielectric heating to simulate the nuclear heat source in studies of the multiphase flow dynamics of volume-boiling systems. For practical reasons, the boiling flow simulation is specified to be contained in a bounded radiation environment such as a microwave oven. The volume-boiling systems are characterized by a spatially varying flow structure. The dielectric properties of the system, therefore, are also space-dependent. Ideally, the microwave power source would provide uniform heating per unit volume of liquid, independent of position, void content and liquid-vapor geometric structure. The uniformity of heating of the liquid phase provided by microwave power is the

major focus of the remainder of this report.

Ideally, we would like to apply Maxwell's equations, with appropriate boundary conditions to obtain the electric field and, hence, the power density distribution, throughout the entire volume-boiling system. If this could be done under a variety of circumstances, then we would simply evaluate the heating uniformity and use parametric studies to optimize conditions. The literature review presented above, however, suggests that on one hand, uniform liquid heating is difficult to achieve in microwave irradiation of homogeneous dielectrics - both in unbounded space and in confined systems such as microwave ovens. On the other hand, analytical methods do not exist to enable us to evaluate the power density distributions in heterogeneous two-phase dielectrics exposed to microwave radiation. Methods are not available even for homogeneous dielectrics exposed in microwave oven radiation fields.

In the absence of the methods to study the general problem outlined above, an alternate approach was adopted. As far as this application of microwave power is concerned, its potential major advantage is that the liquid phase may be heated in a droplet configuration. This is not feasible using low frequency resistive heating. The first part of this work, therefore, is an analysis of the interaction of a microwave radiation field with liquid droplets whose diameters range from microns to centimeter radius. For a given incident electric field intensity, the power absorbed by individual droplets is computed for the above range of diameters. The behavior of various fluid systems is analyzed and compared for uniformity of droplet-averaged power density across the droplet size range of interest. This analysis is made using the scattering theory discussed in Section 2.2. Results are presented in Section 3.1.

In the second part of the analysis reported here, the power density distribution in slab geometry is considered. It is assumed that slabs of single-phase fluids are irradiated by incident plane waves. The power density distribution is computed for various fluid systems, and compared for heating uniformity. The analysis is presented in Section 2.4 and results discussed in Section 3.2.

Preliminary experiments were carried out in a 600 W, 2450 MHz microwave oven in order to investigate the question of heating uniformity. These experiments are described in Chapter IV.

The implications of the analyses with respect to volume-boiling experiments are discussed in Chapter V. The analytical and experimental results are used to select a fluid system whose dielectric properties would be most likely to yield uniform liquid power density distributions when exposed to microwave radiation. A conceptual design of the microwave boiling experimental apparatus is also presented in Chapter V. Chapter VI contains a summary of the report and presents recommendations for an experimental system with which to carry out the proposed volume-boiling simulation studies.

II. ELECTROMAGNETIC WAVE INTERACTIONS WITH MATTER: THEORY

2.1 Introduction

The previous chapter described experiments proposed to investigate the multiphase flow and heat transfer characteristics of volume-boiling fluids which are heated by microwave electromagnetic radiation. It has been assumed in previous studies that the microwave radiation provides a spatially uniform energy source per unit volume of liquid in multiphase flow geometries (Farahat, 1976; Koontz, 1977). It is known, however, that the rate of energy absorption by dielectrics in a microwave electromagnetic field is a function of geometry, dielectric properties, and wavelength of the radiation (Kerker, 1969). At high power density, volume-heated boiling pools exhibit a complex two-phase, liquid-vapor, geometric structure (Ginsberg, 1979). Dispersed droplets, with diameters less than 1 mm, in a vapor continuum may coexist with continuous liquid structures of centimeter scale or greater. This diversity of liquid-vapor structure, together with the expected dependence of microwave heating rate on geometry, led to the conclusion that an analytical study was required to investigate the uniformity of microwave heating in boiling pool systems. This chapter describes the analytical methods that were used in the investigation.

The distribution of heating rate within a dielectric depends upon the electromagnetic field distribution within the material. The field depends not only on the properties of the dielectric but also on the boundary conditions at the walls which confine the entire system. These boundary conditions depend on whether the irradiation takes place in either (i) unbounded space, (ii) a waveguide or (iii) a microwave cavity. Computation of the field distribution in homogeneous dielectrics increases in difficulty in the above order. Indeed, methods do not exist at present to enable one to predict the field distribution and, hence, power density distributions in microwave cavities -even for the case of homogeneous dielectrics. For the case of the heterogeneous two-phase dielectrics of interest here, methods are not available, even for the unbounded space irradiation environments.

Due to the complex two-phase, liquid-vapor geometric structure, simplifying assumptions were made, both with respect to geometry and to the irradiation environment. Two basic problems were chosen for analysis: (i) single spheres exposed to a uniform incident plane polarized radiation field and (ii) slabs

exposed to single-sided and bilateral plane polarized radiation. These problems were chosen in order to investigate two aspects of microwave heating uniformity:

Single spheres.

Previous studies (Mie, 1908; Kerker, 1969) have shown that the rate of energy absorption in spheres exposed to electromagnetic radiation is strongly dependent on sphere radius. Since heating of dispersed droplets is of importance to the boiling studies of interest here, a study of the energy absorption rate of single droplets was initiated. The objective of the study was to determine the uniformity of power density as a function of droplet radius.

The conceptual approach to the problem was to ask: given a microwave electromagnetic field of a given intensity, what is the rate of energy absorbed per unit volume by spheres of liquid of diameters ranging from 10^{-3} mm to 100 mm. The effects of droplet size, dielectric properties and wavelength on the energy absorption efficiency have been investigated. Materials and wavelength combinations were sought in order to obtain uniform volumetric heating rates.

Slab geometry.

The spatial distribution of heating rate within the two-phase boiling fluid is of critical importance to the proposed microwave boiling studies. Previous work (Guy, 1971) has demonstrated that standing waves may be generated in slabs exposed to microwave radiation. The power density distribution in homogeneous slabs exposed to single-sided and bilateral microwave irradiation was investigated. The influences of wavelength material properties and slab width were studied in the investigation of heating uniformity.

Both the sphere and slab geometry problems were investigated for the case of uniform incident plane-polarized electromagnetic radiation. The complexities introduced by confining boundaries were not studied.

This chapter reviews the basic theoretical methods employed in the study of the interaction of "simple" geometries with microwave electromagnetic radiation. Section 2.2 presents definitions of electromagnetic theory terminology used in the report. Section 2.3 discusses the interaction of spherical particles with electromagnetic radiation. The slab irradiation problem is discussed in Section 2.4.

2.2 Definitions of Electromagnetic Quantities of Interest.

In this section relationships are defined and presented for the electromagnetic quantities which are used in the remainder of this paper.

Maxwell's equations in general form are written in Appendix A together with the defining equations for the material properties of specific conductance, σ; electrical inductive capacity (or permittivity) ε; magnetic inductive capacity (or permeability), μ. In absorbing media the permittivity and the permeability are complex quantities.

The complex permittivity is defined by

$$\varepsilon^* = \varepsilon' - j\,\varepsilon'' \tag{2.1}$$

and the complex permeability is

$$\mu^* = \mu' - j\,\mu'' \tag{2.2}$$

The complex relative permittivity and permeability are, respectively,

$$k^* = \frac{\varepsilon^*}{\varepsilon_o} = k' - j\,k'' \tag{2.3}$$

$$k_m^* = \frac{\mu^*}{\mu_o} = k_m' - j\,k_m'' \tag{2.4}$$

The "loss tangent" is defined by

$$\tan\,\delta = \frac{\varepsilon''}{\varepsilon'} = \frac{k''}{k'} \tag{2.5}$$

The one-dimensional wave equation for the electric field may be written as

$$\frac{\partial^2 \vec{E}}{\partial x^2} = \varepsilon^*\,\mu^*\,\frac{\partial^2 \vec{E}}{\partial t^2} \tag{2.6}$$

The solution to this equation is of the form

$$\vec{E} = \vec{E}_o \exp (j\omega t - \gamma^* x) \tag{2.7}$$

The quantity γ^* is the "complex propogation factor" defined by

$$\gamma^* = j\omega (\varepsilon^* \mu^*)^{1/2} \tag{2.8}$$

$$= \alpha + j\beta$$

The "index of refraction" of the dielectric medium is defined by

$$n = \frac{\lambda}{\lambda_m} = \frac{\lambda}{2\pi} \beta \tag{2.9}$$

The "index of absorption" is given by

$$k = \frac{\alpha \lambda_m}{2\pi} = \frac{\alpha}{\beta} \tag{2.10}$$

and the complex index of refraction is

$$m^* = n (1 - j k)$$

$$= n - jn'$$

$$= (\varepsilon^*)^{1/2} \tag{2.11}$$

where n' is the imaginary part of the complex index of refraction. The complex propogation factor then may be written as

$$\gamma^* = j \frac{2\pi}{\lambda} m^* \tag{2.12}$$

2.3 Electromagnetic Wave Interactions with Absorbing Spheres.

Consider a particle which is exposed to a uniform, plane-polarized beam of electromagnetic radiation, as shown schematically in Figure 2.1. The physics of energy scattering and absorption by the particle is governed by the solution to Maxwell's equations. The general theory of scattering of radiation by spherical particles is found in classical works on electromagnetic theory (Mie, 1908; Stratton, 1941; Kerker, 1969). A brief outline of the theory is presented in Appendix A of this report.

The quantities of interest in the present analysis of microwave absorption are: (i) the energy absorption rate, P, of a single particle, and (ii) the power density, Q''', or power absorbed by a single particle per unit volume of particle. These quantities are defined by the relationships

$$P = \phi_{INC} \cdot C_{ABS} = {}_{INC}\, Q_{ABS} \cdot A \tag{2.13}$$

and

$$Q''' = \frac{P}{V} = \phi_{INC}\ Q_{ABS}\ \frac{A}{V} \tag{2.14}$$

$$= \frac{3}{4a}\ \phi_{INC}\ Q_{ABS} \tag{2.15}$$

where C_{ABS} and Q_{ABS} are the absorption cross-section and absorption efficiency, respectively. The incident energy flux is given by (Kraus, 1953)

$$\phi_{INC} = \frac{1}{2} \sqrt{\frac{\varepsilon_o}{\mu_o}}\ E_o^{\,2} \tag{2.16}$$

In the present work, a dimensionless power density, ψ, is used t resent the droplet power density distribution information. This quantity is fined as

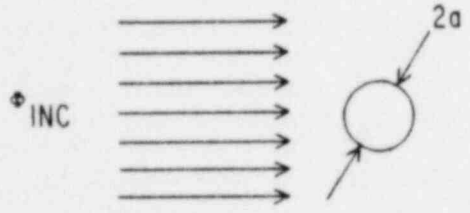

- Droplet Radius, a
- Frontal Area, A
- Volume, V
- Absorption Cross-Section, C_{ABS}
- Absorption Efficiency, Q_{ABS}
- Incident Energy Flux, Φ_{INC}

- Power Absorbed

$$P = \Phi_{INC} \cdot C_{ABS}$$

$$= \Phi_{INC} \cdot Q_{ABS} \cdot A$$

- Power Density

$$Q''' = \frac{P}{V}$$

$$= \Phi_{INC} \cdot Q_{ABS} \cdot \frac{A}{V}$$

$$= \frac{3}{4} \Phi_{INC} \cdot \frac{Q_{ABS}}{a}$$

Figure 2.1 Schematic of Particle Exposed to Plane Wave Incident Beam of Radiation. (BNL Neg. No. 12-816-80)

$$\psi(a) = \frac{P(a)/V(a)}{P(a_o)/V(a_o)} = \frac{Q_{ABS}(a)/a}{Q_{ABS}(a_o)/a_o} \tag{2.17}$$

where a_o is a reference droplet radius.

The absorption as well as scattering and extinction cross-sections are obtained from infinite series solutions of Maxwell's equations in spherical coordinates. A brief summary of the solution method, together with the series representations for the cross-sections are also presented in Appendix A.

In general, the series relationships must be evaluated for the cross-sections. For the case of "sufficiently small" particle radius, however, the infinite series simplifies to the Rayleigh approximation (Kerker, 1969). The absorption efficiency then becomes

$$Q_{ABS} = \text{Im} \left\{ - \frac{8\pi a}{\lambda} \quad \frac{m^{*2} - 1}{m^{*2} + 2} \right\} \tag{2.18}$$

where m* is the complex index of refraction. Using this relationship together with Equation (2.14), the particle power density becomes

$$Q''' = \frac{3}{4} \Phi_{INC} \cdot \text{Im} \left\{ - \frac{8\pi}{\lambda} \quad \frac{m^{*2} - 1}{m^{*2} + 2} \right\} \tag{2.19}$$

The power density of "small" particles, therefore, is independent of particle size.

Every material, therefore, is characterized by a range of particle size within which their power density is independent of diameter. This result is of significance in the present work, since it implies that uniform heating of liquid droplets independent of diameter may be possible.

A computer code DILISCA* (DIfferential LIght SCAtterin~) was employed to evaluate the cross-sections from the infinite series solution to Maxwell's equations.

* Computer code developed by Science Spectrum Inc. of Santa Barbara, Calif.

2.4 Electromagnetic Wave Interactions with Absorbing Slabs.

2.4.1 Sources of Identical Frequency.

Consider the slab of dielectric medium shown in Figure 2.2, irradiated either from one side only or irradiated bilaterally. Two analytical problems were studied: (i) the general problem with boundary effects for both single-sided and bilateral irradiation and (ii) bilateral irradiation of a slab in which internal boundary reflections are not considered.

The electric field within the slab depends on the relative orientation of the electric and magnetic field vectors, the relative phases of the incident plane waves, the dielectric properties of the slab, the wavelength and on the slab width. The electric field within the slab, when irradiated from the left side only, is due to the interaction of two waves, one which is transmitted across the left surface, and the other reflected internally from the right surface. The field within the slab is given by (see Appendix D)

$$\frac{E}{E_o} = t_o e^{j\omega t} \left(e^{-\gamma_2^* x} + r_1 e^{\gamma_2^* x}\right) \tag{2.20}$$

If the slab is irradiated bilaterally with sources of equal frequency and strength, then the field may be computed by superposition. The resulting field distribution in the slab is given by (see Appendix D)

$$\frac{E}{E_o} = e^{j\omega t} \left\{ e^{-\gamma_2^* x} + e^{(j\omega\phi + \gamma_2^* x')} + r_1 \left[e^{\gamma_2^* x} + e^{-(j\omega\phi + \gamma_2^* x')} \right] \right\} \tag{2.21}$$

where $x' = x - \ell$ and ℓ is the slab thickness. The time-average mean-square electric field is computed using the averaging technique discussed in Appendix B. The result (see Appendix D for details) is

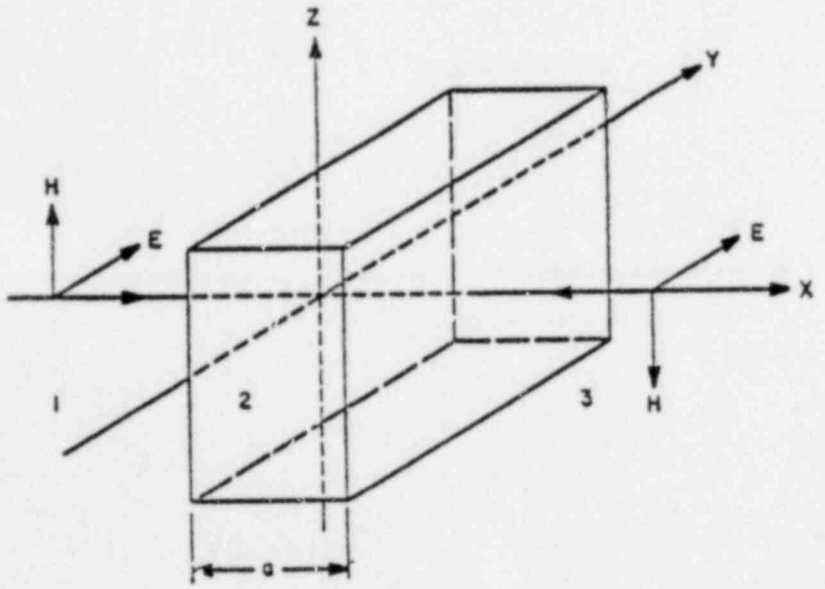

Figure 2.2 Schematic of Slab Exposed to Plane Wave Normally Incident Radiation. (BNL Neg. No. 11-533-79)

$$\frac{\overline{E^2}}{E_o^2} = \cosh(2\delta x) + 2\cos^2 \xi x - 1 \qquad (2.22)$$

2.4.2 Sources of Different Frequency.

Consider a slab irradiated bilaterally with sources of different frequency, as represented schematically in Figure 2.2. This problem is discussed in Appendix C, where the general solution for the field distribution in the slab is given. For the special case where the frequencies are only slightly different, it is shown that the field is given by

$$\frac{\overline{E^2}}{E_o^2} = \cosh(2\delta x) \qquad (2.23)$$

III. THEORETICAL PREDICTIONS

3.1 Introduction.

This chapter presents the results of calculations of microwave interactions with absorbing dielectric liquid spheres and liquid slabs. In these calculations geometric and material properties are varied and the effects on heating rate, or power density, are studied as a function of these parameters.

Results for microwave interactions with spheres are presented in Section 3.2. Verification of the DILISCA code used in these calculations is discussed in Section 3.2.1. General features of the predictions are discussed in Section 3.2.2 using water as the dielectric material. Sections 3.2.3 and 3.2.4 present detailed results for water and ethyl alcohol, respectively. A parametric study which was performed to determine the combination of dielectric properties which would lead to uniform droplet heating is presented in Section 3.2.5. In Section 3.2.6 it is shown how selected polar and non-polar molecular mixtures can be tailored to provide uniform droplet power density over a wide range of droplet size.

Slab geometry results are presented in Section 3.3. Calculational results are discussed for cases of single-sided and bilateral microwave irradiation of slabs. For the case of bilateral irradiation, results are presented for sources of identical frequency, and also for sources of two different frequencies. The spatial uniformity of heating rate is studied as a function of dielectric properties, geometry and wavelength.

3.2 Interaction of Microwaves With Spherical Dielectrics.

3.2.1 Code Verification.

The computer code DILISCA was obtained, modified and verified for the current application. DILISCA evaluates the scattering, absorption and extinction coefficients and cross-sections for given wavelength and dielectric properties. As a result of additional programming work done on the code, it now also computes the dimensionless sphere power density, defined by Equation (2.14).

DILISCA was verified by comparison with the Tables of Scattering Functions for spheres (U.S. National Bureau of Standards, 1949) using a range of radii and dielectric properties. Code calculations agreed with tabular results within the number of significant digits presented in the tables.

A comparison was also made between DILISCA calculations and the results of Kerker (1969) [p. 121] for $m^* = 1.29 - 0.0472j$, for a 100 mm wavelength. This comparison is presented in Figure 3.1.

3.2.2 General Features.

The general features of the case to be discussed below, for water, are applicable to other material dielectric properties and wavelengths, although the functional dependance on 'a', the radius of the droplet, is different for other material.

Water, being a simulant fluid of immediate interest to the volume-boiling work, was investigated over a range of wavelengths, using index of refraction data extrapolated from Collie (1948) and Lane (1952). Figure 3.2a shows the behavior of the absorption efficiency Q_{ABS}, as a function of radius for a fixed microwave wavelength of 100 mm. Figure 3.2b presents the dimensionless power density as a function of radius, where the power density is normalized with that of a 50 mm droplet.

Results are presented for a microwave wavelength of 100 mm, corresponding to standard commercially available microwave equipment. From Figure 3.2, it is observed that there are three regimes of microwave-droplet interaction. In the region from $a = 0$ to $a \simeq 5$ mm the interaction efficiences are extremely low, and the rate of energy absorption is also very low. The region from $a \simeq 5$ mm to $a \simeq 30$ mm is a resonance region, characterized by rather large variations in the absorption efficiencies with radius. This is apparent in Figure 3.2b which shows the correspondingly large variations in heating rate, with peak heating rates at about 10 mm radius of nearly two orders of magnitude greater than a 5 mm "droplet". In the range $a > 30$ mm, the efficiencies are nearly constant and, consequently, the rates of energy absorption (proportional to Q_{ABS}/a) per unit "droplet" volume decrease with increasing radius.

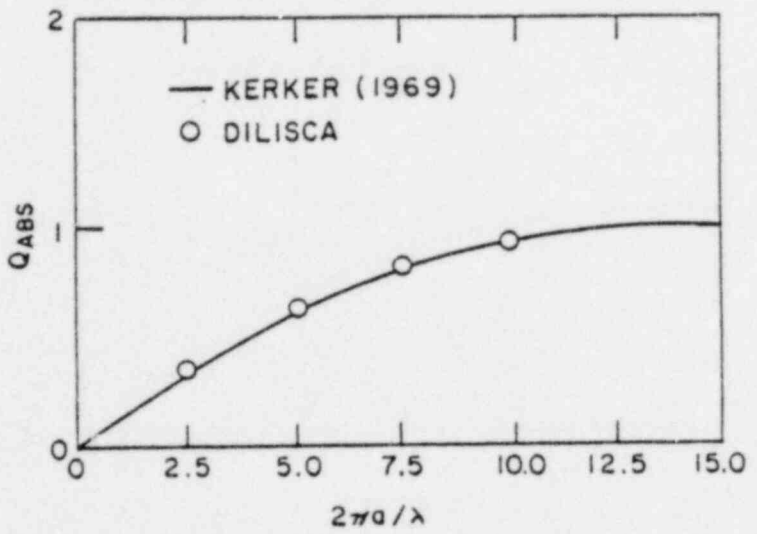

Figure 3.1 Comparison of DILISCA Results with Kerker (1969).

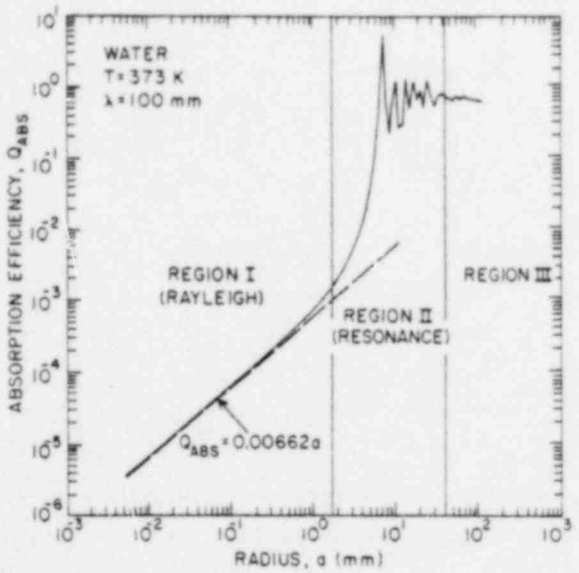

(a)

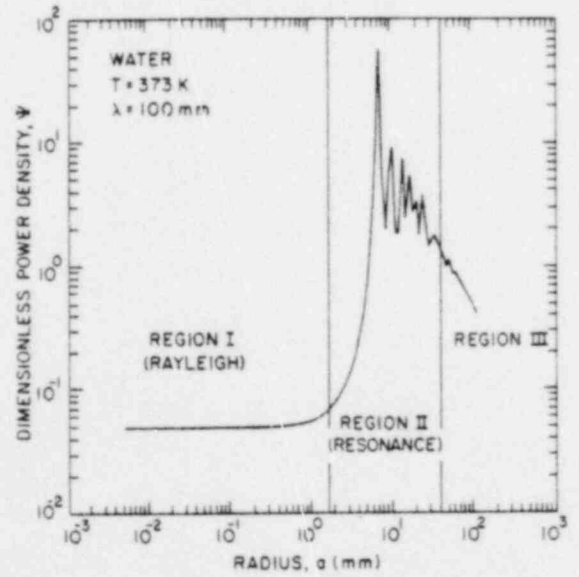

(b)

Figure 3.2 Absorption Efficiency (a) and Power Density (b) for Water Spheres: λ = 100 mm; T = 373 K.
(BNL Neg. No. 12-822-80; 12-594-80)

A finer look at the region corresponding to a = 0 to a $\simeq$ 1 mm shows a linear behavior of Q_{ABS} with radius, as shown in Figure 3.2a. This behavior is predicted by Equation (2.17) and is plotted in Figure 3.2a. The power density function , shown in Figure 3.2b, exhibits a constant behavior in this linear region of absorption efficiency. Water droplets with radii up to 1 mm would be heated with the same power density when exposed to microwaves of 100 mm wavelength. This range of droplet radius is characterized as Region I in Figure 3.2.

Figure 3.3 presents a closer look at the resonance region, characterized as Region II of Figure 3.2. Both absorption efficiency and power density display peaks at a = 1/7 λ, 1/10 λ, 1/14 λ over the range of radius plotted in Figure 3.3. Region III, at least up to a = 100 mm, is characterized by nearly constant absorption coefficient.

3.2.3 Results for Water.

DILISCA calculations were performed for several combinations of wavelength and water temperature. Table 3.1 summarizes the range of parameters and presents the complex index of refraction for each combination of temperature and wavelength.

Values for the complex dielectric properties of water over a range of wavelengths and temperature are presented by Gunn (1954) and Lane (1952). The available information was developed into a self-consistent data set for water temperatures from 293 - 373 K and wavelengths from 1- 300 mm. Very little data exists in the literature for dielectric properties of water approaching boiling ($\sim$ 373 K). Most of the dielectric property data for temperature greater than 353 K were extrapolated. It is felt that this extrapolation is reasonable as long as the temperatures is somewhat less than the boiling point. The data for real and imaginary indices of refraction are presented in Figures 3.4 - 3.8. The extrapolation regions are presented with each set of data.

The effects of wavelength and fluid temperature on droplet energy absorption efficiency and power density were studied. Results of the parametric study are presented in Figures 3.9 - 3.11.

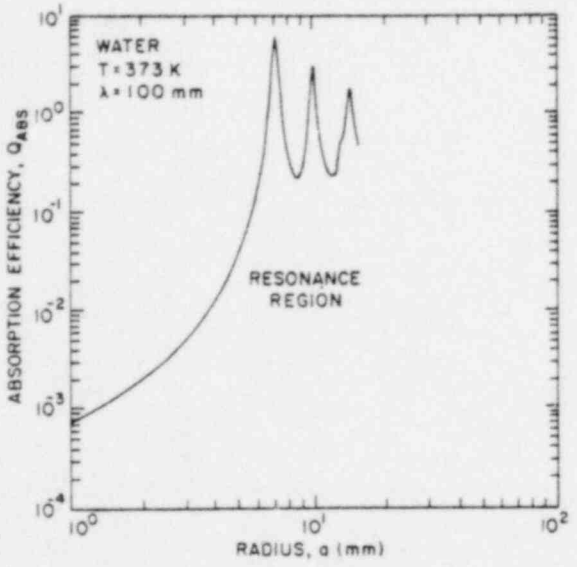

(a)

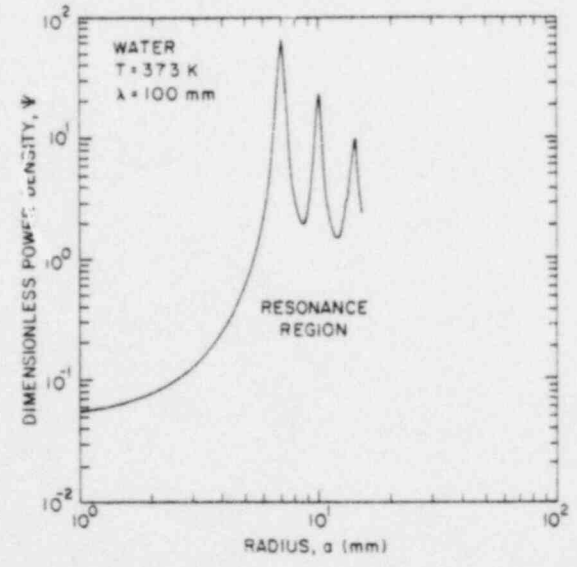

(b)

Figure 3.3 Resonance Region Absorption Efficiency (a) and Power Density (b) for Water Spheres: λ = 100 mm; T = 373 K. (BNL Neg. No. 12-590-80; 12-586-80)

Table 3.1 - INDICES OF REFRACTION USED IN CALCULATIONS: WATER

T(K) λ(mm)	293	323	348	373
12.7	6.25 - 2.86j	7.26 - 2.11j	7.35 - 1.52j	7.40 - 0.85j
32.1	8.08 - 1.97j	8.15 - 1.05j	7.82 - 0.67j	
100.0	8.83 - 0.74j	8.28 - 0.35j	7.78 - 0.21j	7.1 - 0.17j
200.0	9.80 - 0.50j	8.6 - 0.2 j	7.8 - 0.2 j	
300.0			7.8 - 0.2 j	

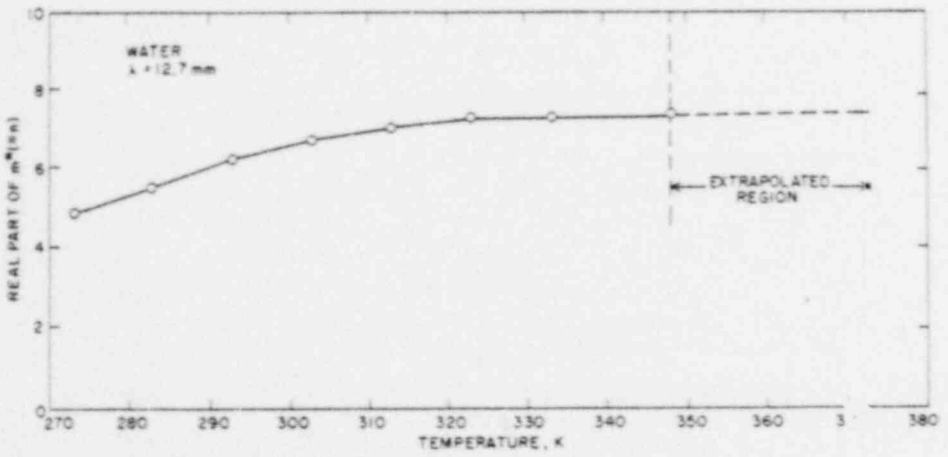

(a)

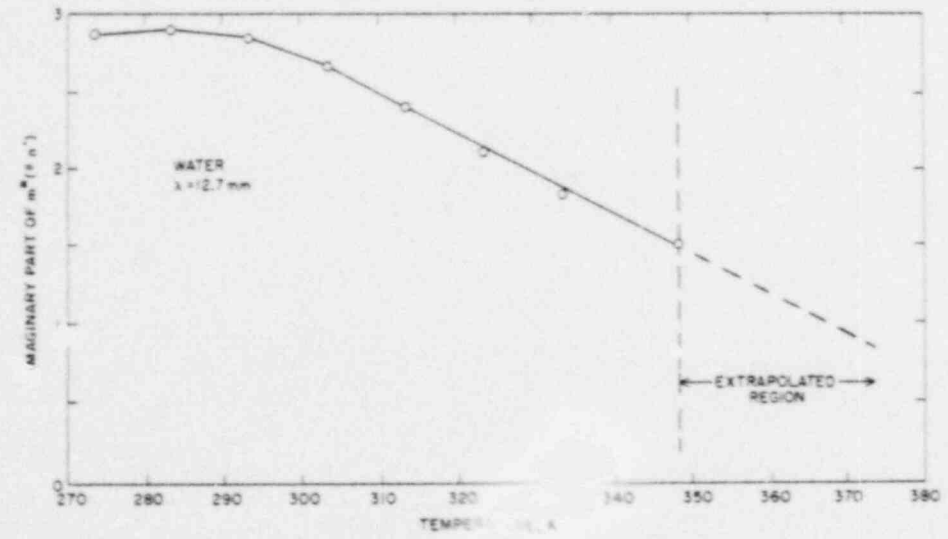

(b)

Figure 3.4 Real (a) and Imaginary (b) Indices of Refraction for Water: λ = 12.7 mm. (BNL Neg. No. 12-808-80; 12-809-80)

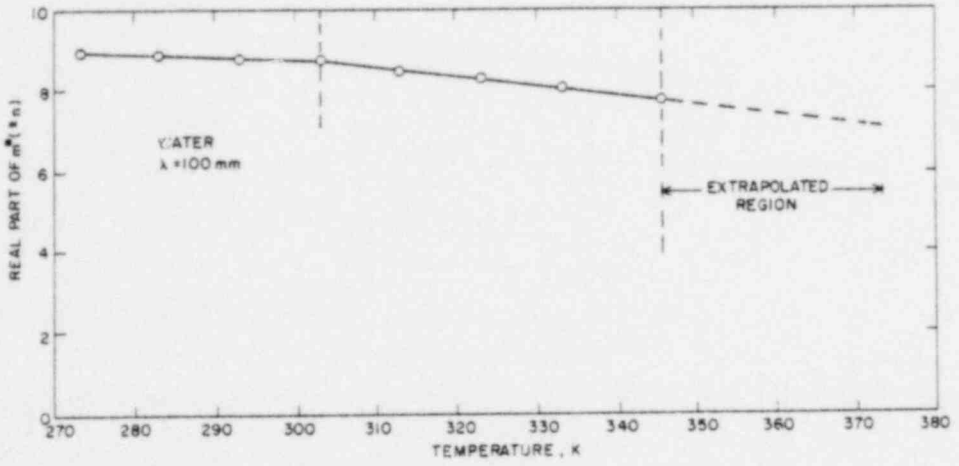

(a)

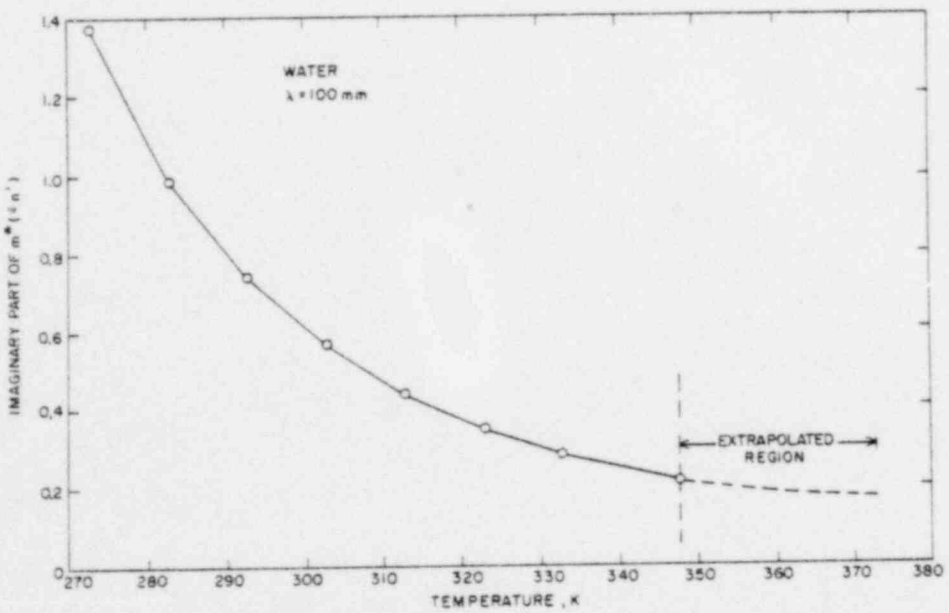

(b)

Figure 3.5 Real (a) and Imaginary (b) Indices of Refraction for Water: λ = 100 mm. (BNL Neg. No. 12-605-80; 12-604-80)

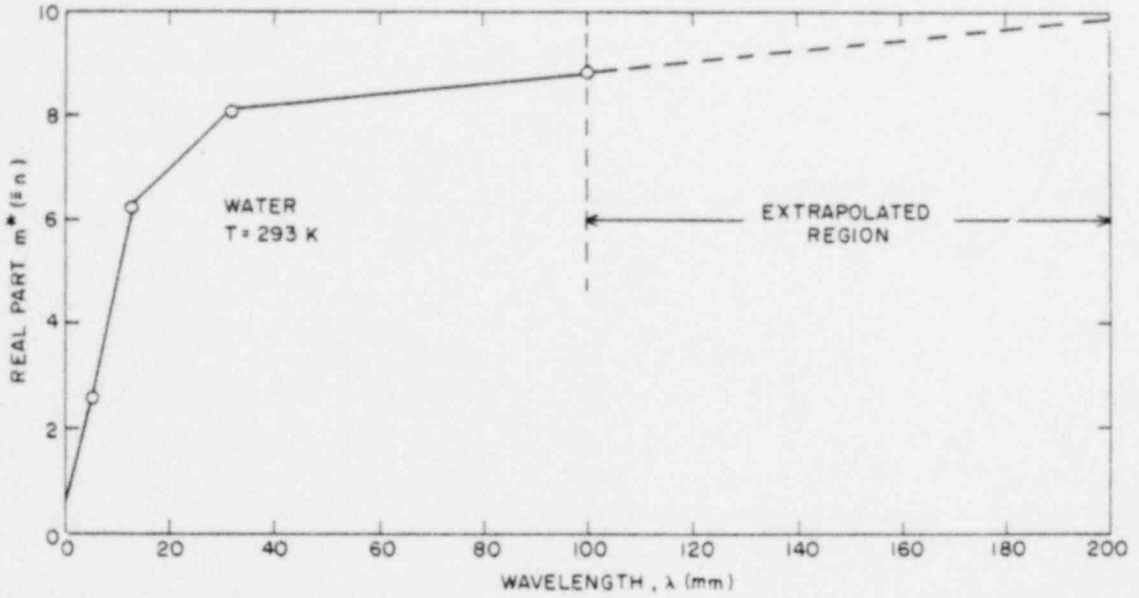

(a)

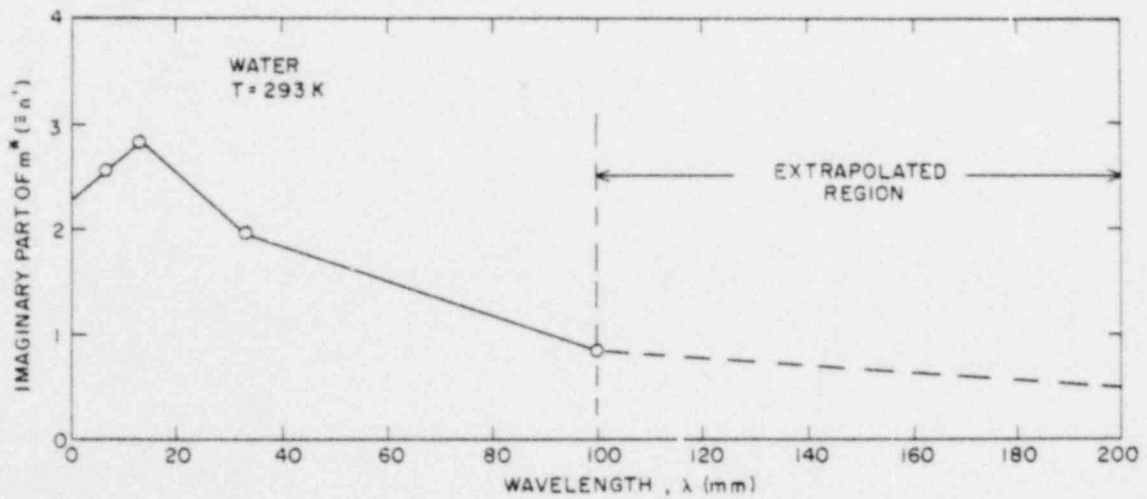

(b)

Figure 3.6 Real (a) and Imaginary (b) Indices of Refraction for Water: T = 293 K. (BNL Neg. No. 12-806-80; 12-804-80)

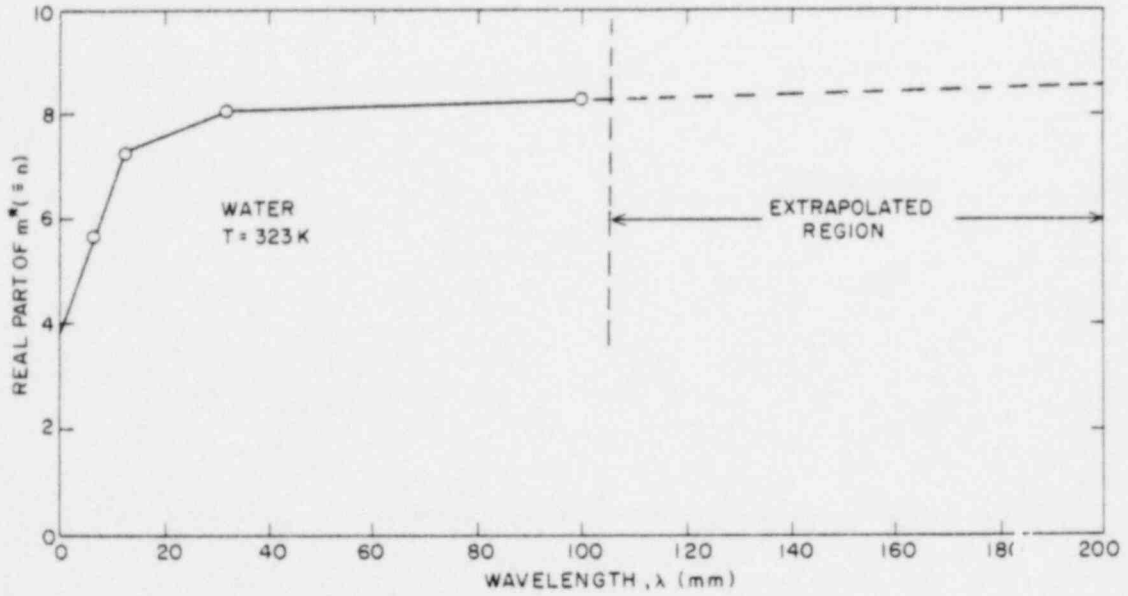

(a)

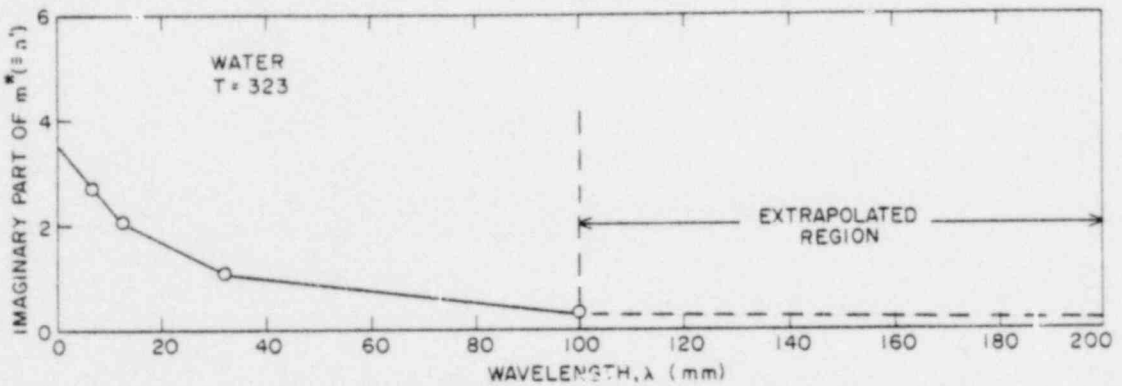

(b)

Figure 3.7 Real (a) and Imaginary (b) Indices of Refraction for Water: T = 323 K. (BNL Neg. No. 12-601-80; 12-599-80)

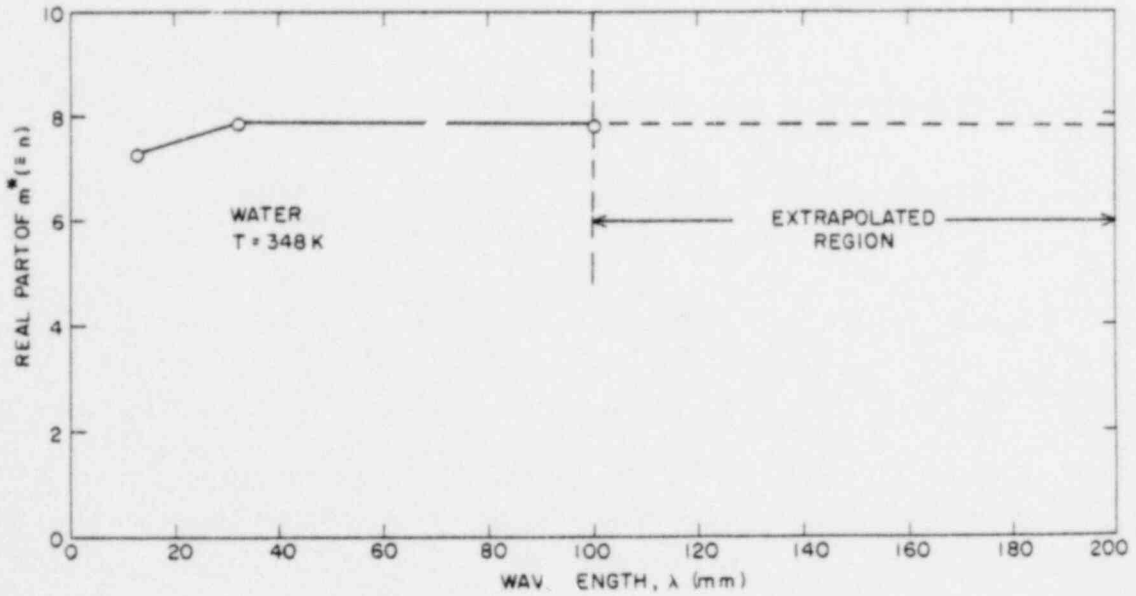

(a)

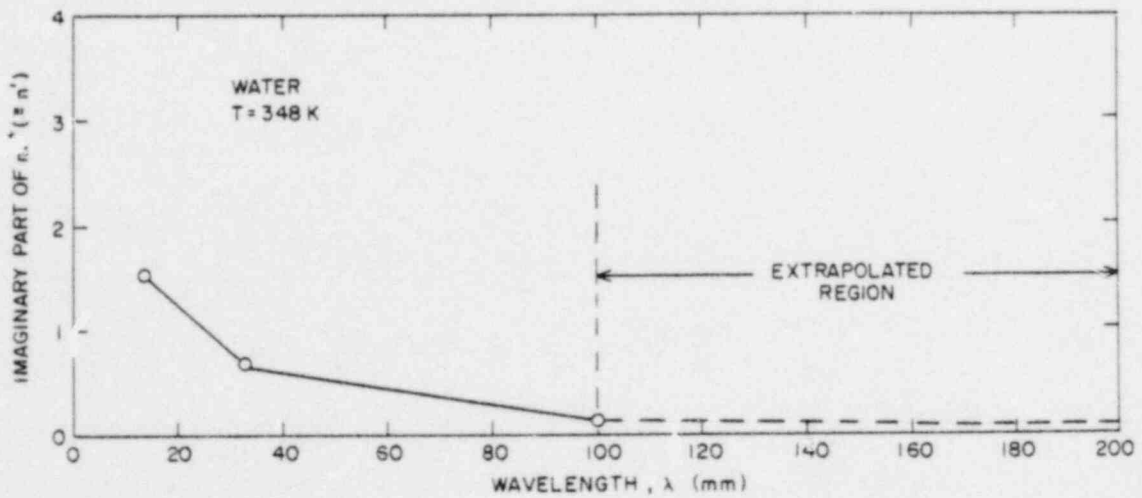

(b)

Figure 3.8 Real (a) and Imaginary (b) Indices of Refraction for Water: T = 348 K. (BNL Neg. No. 12-598-80; 12-600-80)

3.2.3.1 Effects of Wavelength.

Figures 3.9 and 3.10 show the influence of incident E-M wavelength on the droplet energy absorption characteristics.

Figures 3.9a, 3.10a and 3.10c show that the energy absorption efficiency for water droplets of radii less than 10 mm increases with decreasing wave length. It is much easier, therefore, to transfer energy from a source of E-M energy to millimeter water droplets at wavelengths of order 10 millimeters.

The linear region of energy absorption efficiency increases with wavelength. This is best observed on the power density distribution plots. Figure 3.9b shows that at 373 K, the power density is constant for droplets with radii up to 1 mm for λ = 100 mm. At a wavelength of 12.7 mm the power density is constant only up to 0.1 mm. Similar results are presented in Figure 10 for 348 K water. For λ = 300 mm the power density is reasonably uniform up to a radius of approximately 1 mm. For λ = 12.7 mm it is constant only up to approximately 0.1 mm.

The above results clearly indicate that it is possible to extend the regime of constant power density to larger radius droplets through use of longer wavelength microwaves. A wavelength of 100 mm appears to be optimal from the standpoint of providing a wide regime of constant power density. Going from 100 to 300 mm provides no significant increase in the domain of constant power density. Along with the larger domain of constant power density provided by the 100 mm wavelength, however, one finds that centimeter-size droplets are much more efficient energy absorbers than millimeter radius droplets. The power density of centimeter-scale water droplets are two orders of magnitude greater than that of the millimeter droplets.

3.2.3.2 Effects of Water Temperature.

Computational results for the effect of temperature on the power density distributions are presented in Figure 3.11 for 100 mm wavelengths. Similar results have been obtained for λ = 200 mm.

The results indicate that water temperature has no significant influence on

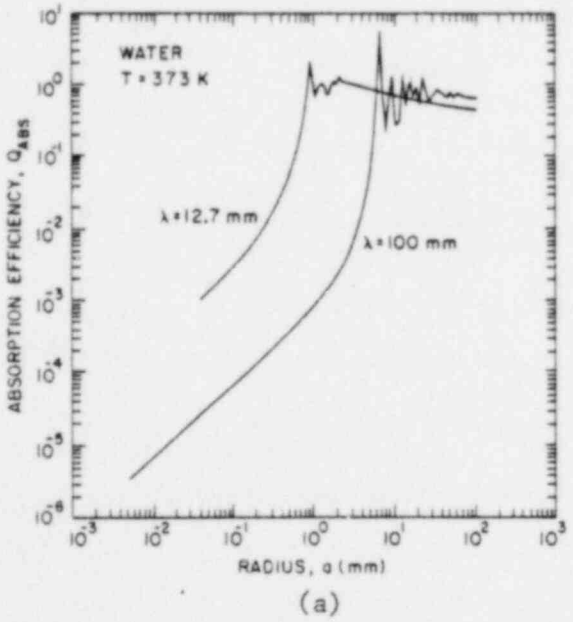

(a)

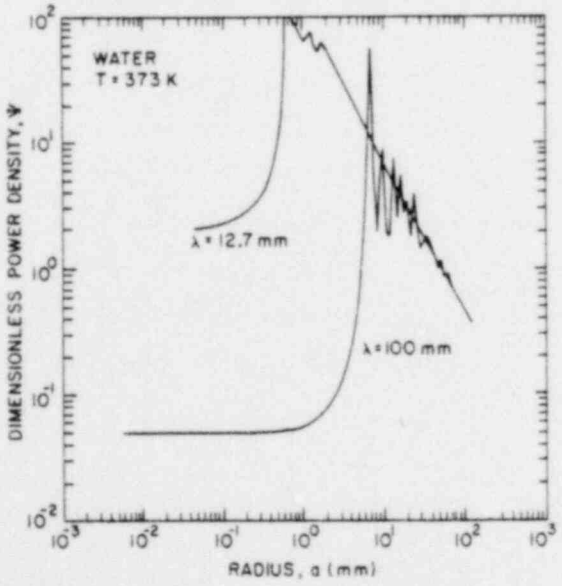

(b)

Figure 3.9 Absorption Efficiency (a) and Power Density (b) for Water Spheres: λ = 12.7 and 100 mm; T = 373 K.
(BNL Neg. No. 12-596-80; 12-595-80)

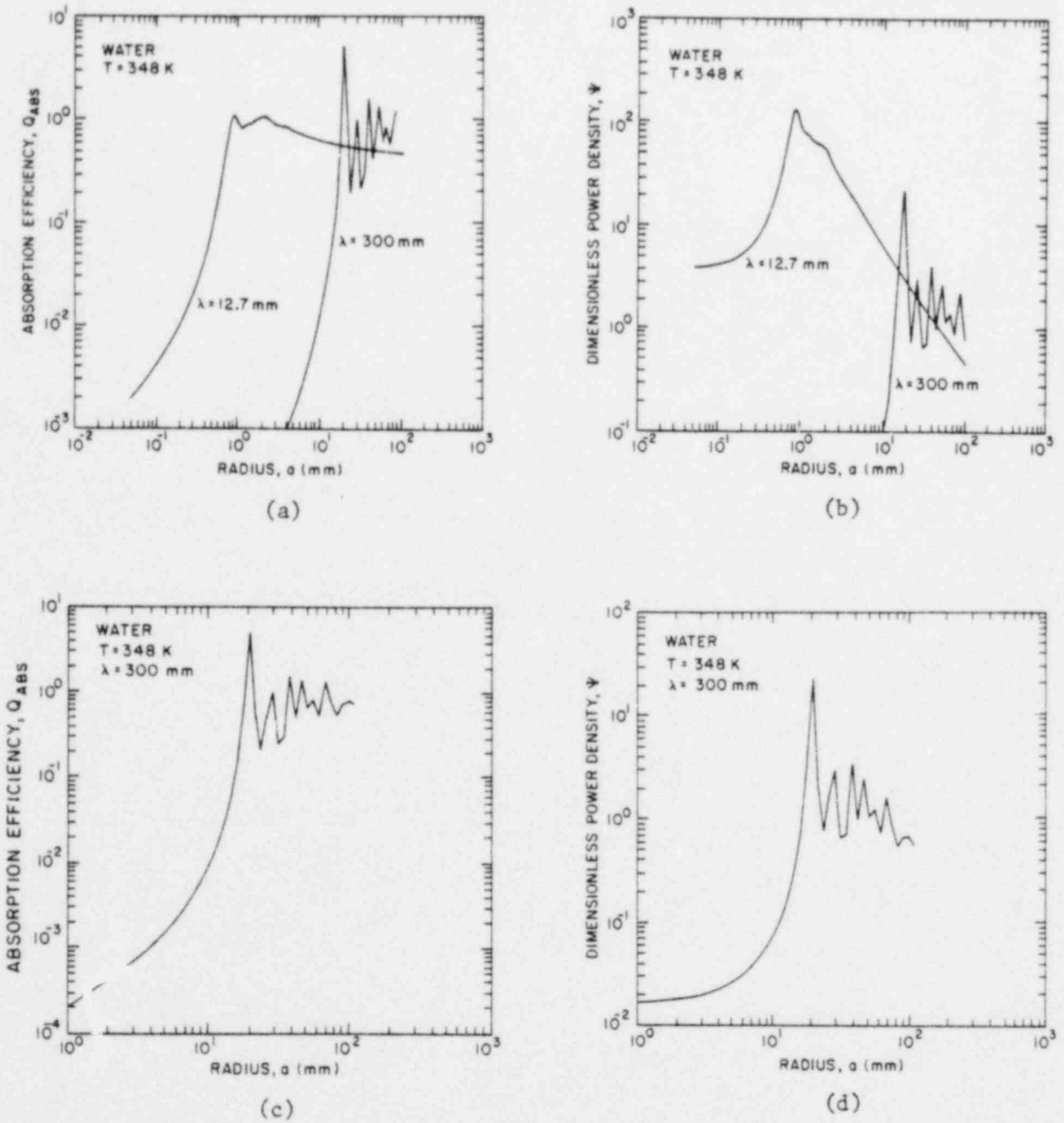

Figure 3.10 Absorption Efficiency (a,c) and Power Density (b,d) for Water Spheres: λ = 12.7 and 300 mm; T = 348 K.
(BNL Neg. No. 12-583-08; 12-582-80; 12-589-80; 12-584-80)

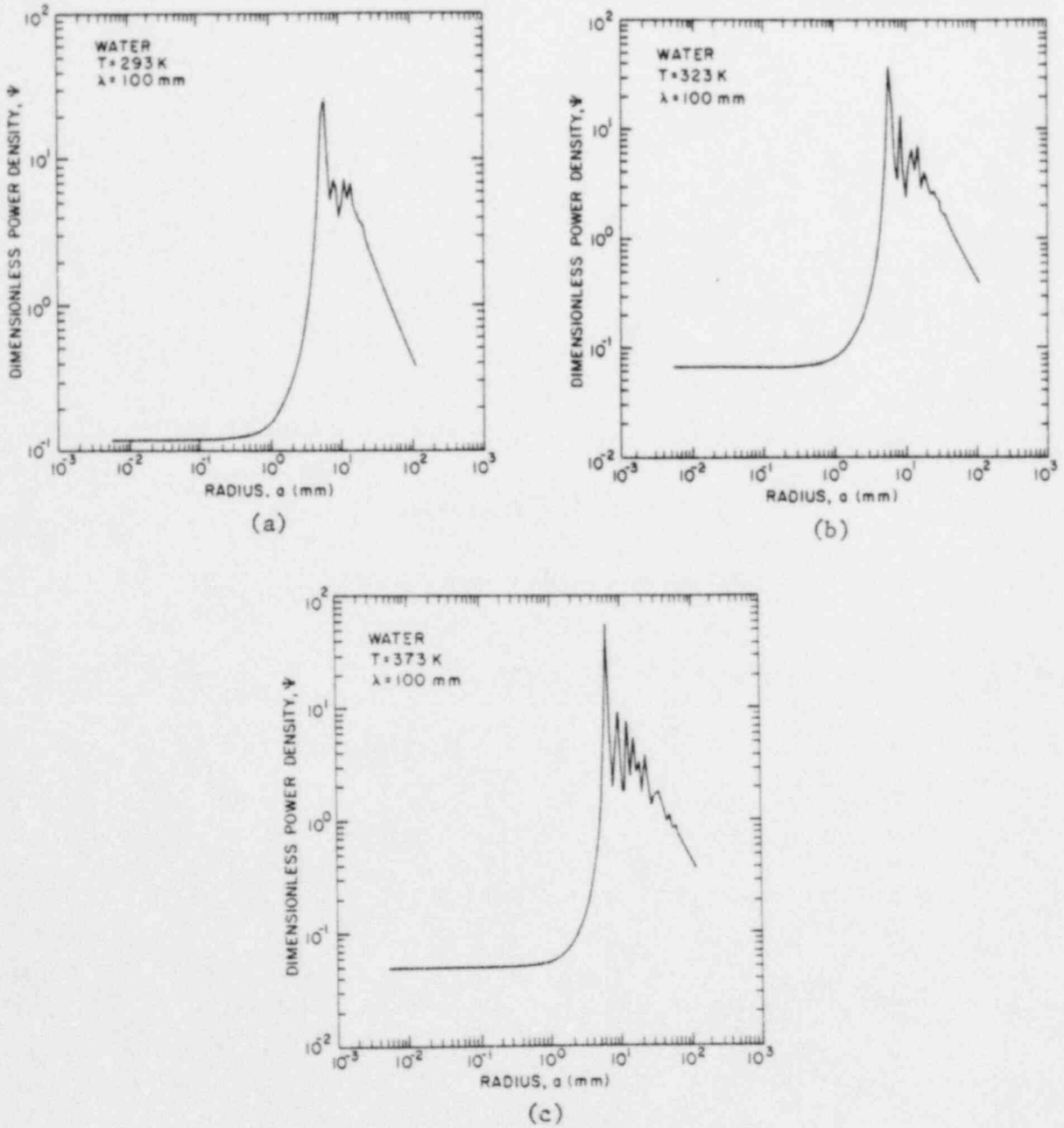

Figure 3.11 Power Density for Water Spheres: λ 100 mm; T = (a) 293 K, (b) 323 K, (c) 373 K.
(BNL Neg. No. 12-590-80; 12-593-80; 12-818-80)

the dominant features of the power density distributions. It is observed, however, that the resonance peaks increase in magnitude and the resonance region width (with respect to radius) increases with increasing temperature. In addition, the regime of constant power density increases somewhat with temperature. These conclusions also apply for λ = 200 mm.

3.2.3.3 Summary of Water Results.

The power density distributions presented above for water suggest that uniform heating cannot be accomplished in a system which contains both millimeter and centimeter-scale water droplets. Water, therefore, appears to be a poor candidate for a simulant fluid to be used in the volume-boiling studies discussed in Chapter I. This is due to the fact that the energy absorption rate per unit volume of liquid varies by up to two orders-of-magnitude over the droplet radius range of interest in the proposed experimental simulation, for the range of microwave wavelengths and temperatures considered above.

3.2.4 Results for Ethyl Alcohol (Ethanol).

Ethyl alcohol was studied because its dipole moment is smaller than that of water, which results in lower values of the real part of the index of refraction. It was felt that reduction of the real part of m^* would result in a more uniform power density distribution compared with water, since the resonant coupling would not be as strong.

Data for the dielectric properties of ethyl alcohol were obtained from Lane (1952), Von Hippel (1954) and Westphal (1978). The data used in the calculations are presented in Figures 12 and 13. Note that while the dependence of m^* on wavelength is similar to water, the temperature dependence is not. Both n and k increase with temperature.

DILISCA calculations were performed for the range of temperatures and wavelengths shown in Table 3.2 along with the associated indices of refraction. As with water, extrapolations were made up to the normal boiling point of ethyl alcohol (351.4 K). Computational results are presented in Figures 3.14 and 3.15.

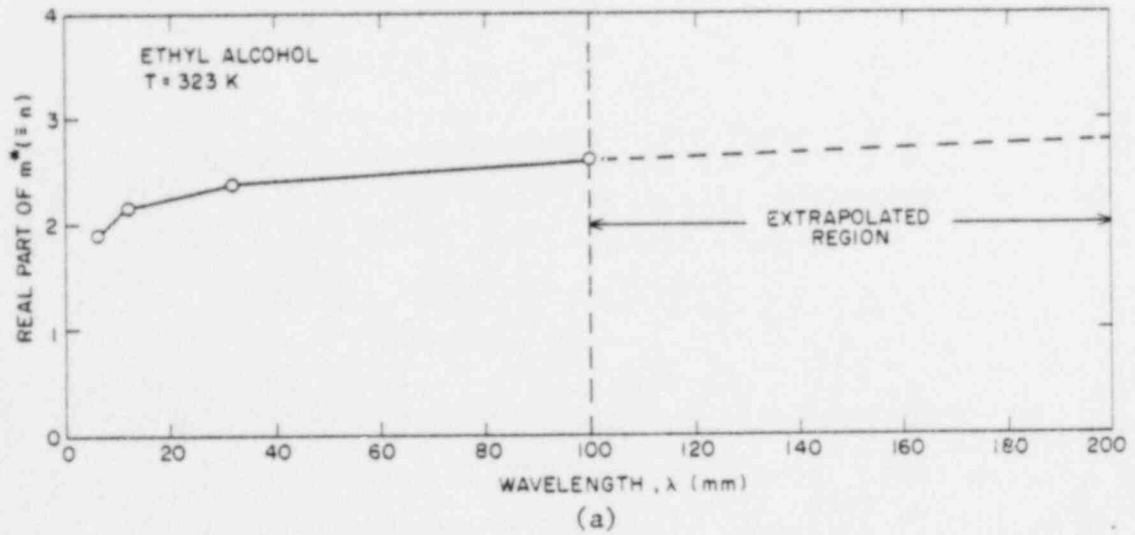

(a)

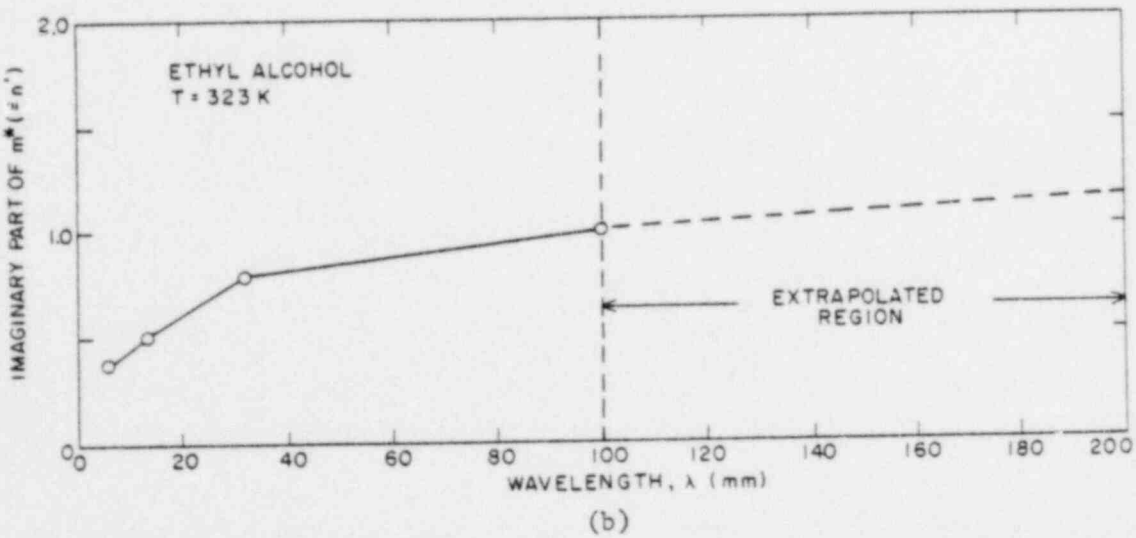

(b)

Figure 3.12 Real (a) and Imaginary (b) Indices of Refraction for Ethyl Alcohol: T = 323 K. (BNL Neg. No. 12-597-80; 12-602-80)

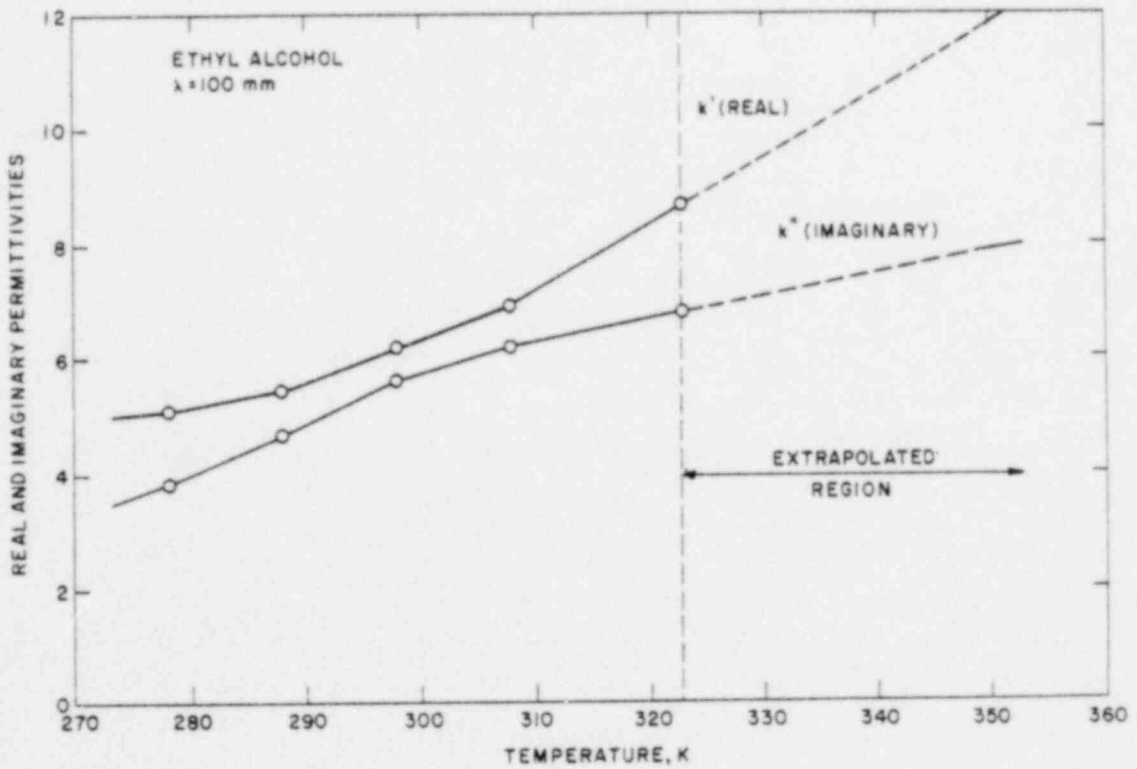

Figure 3.13 Real and Imaginary Permittivities for Ethyl Alcohol: λ = 100 mm. (BNL Neg. No. 12-807-80)

Table 3.2 - INDICES OF REFRACTION USED

IN CALCULATIONS: ETHYL ALCOHOL

T(K) λ(mm)	298	323	348
12.4	2.10 - 0.39j	2.16 - 0.53j	
32.1	2.21 - 0.56j	2.40 - 0.81j	
100.0	2.71 - 1.05j	3.14 - 1.08j	3.58 - 1.09j
200.0		2.8 - 1.3j	

3.2.4.1 Effects of Wavelength.

A typical plot of absorption efficiency for ethyl alcohol is shown in Figure 3.14a. The characteristic feature of this result is the smooth transition from the linear regime of Q_{ABS} into the non-linear regime. A pronounced resonance region is not observed for ethyl alcohol. This result is typical for all wavelengths studied.

Figures 3.14b - 3.14d show the power density distributions for wavelengths varying from 32.1 to 200 mm. Note that the regime of constant power density increases with increasing wavelength. For λ = 200 mm and at 323 K, this region extends out to almost 5 mm droplet radius. The power density variation over the range of droplet radius from zero to 50 mm is approximately a factor of 3 for λ = 200 mm and more than one order of magnitude for λ = 32.1 mm. Clearly the variation in power density for ethyl alcohol droplets is much less pronounced than for water droplets exposed to the same wavelength radiation.

3.2.4.2 Effects of Temperature.

The effects of temperature on the power density distribution of ethyl alcohol are shown in Figure 3.15 for a fixed wavelength of λ = 100 mm. At the higher temperatures the variation in power density is more pronounced. Results not shown here also indicate that the resonance region becomes more pronounced with increasing temperature. This is, however, a secondary side effect.

3.2.4.3 Summary of Ethyl Alcohol Results.

The results clearly demonstrate that ethyl alcohol droplets are heated significantly more uniformly than water droplets exposed to the same frequency. The physical parameter which is most responsible for this behavior is the real part of the complex index of refraction. The real part of m^* is in the range 2-3 for ethyl alcohol and in the range of 7-9 for water at comparable temperatures and exposed to similar wavelength radiation.

3.2.5 Parametric Studies.

A series of calculations was performed to determine the range of real and

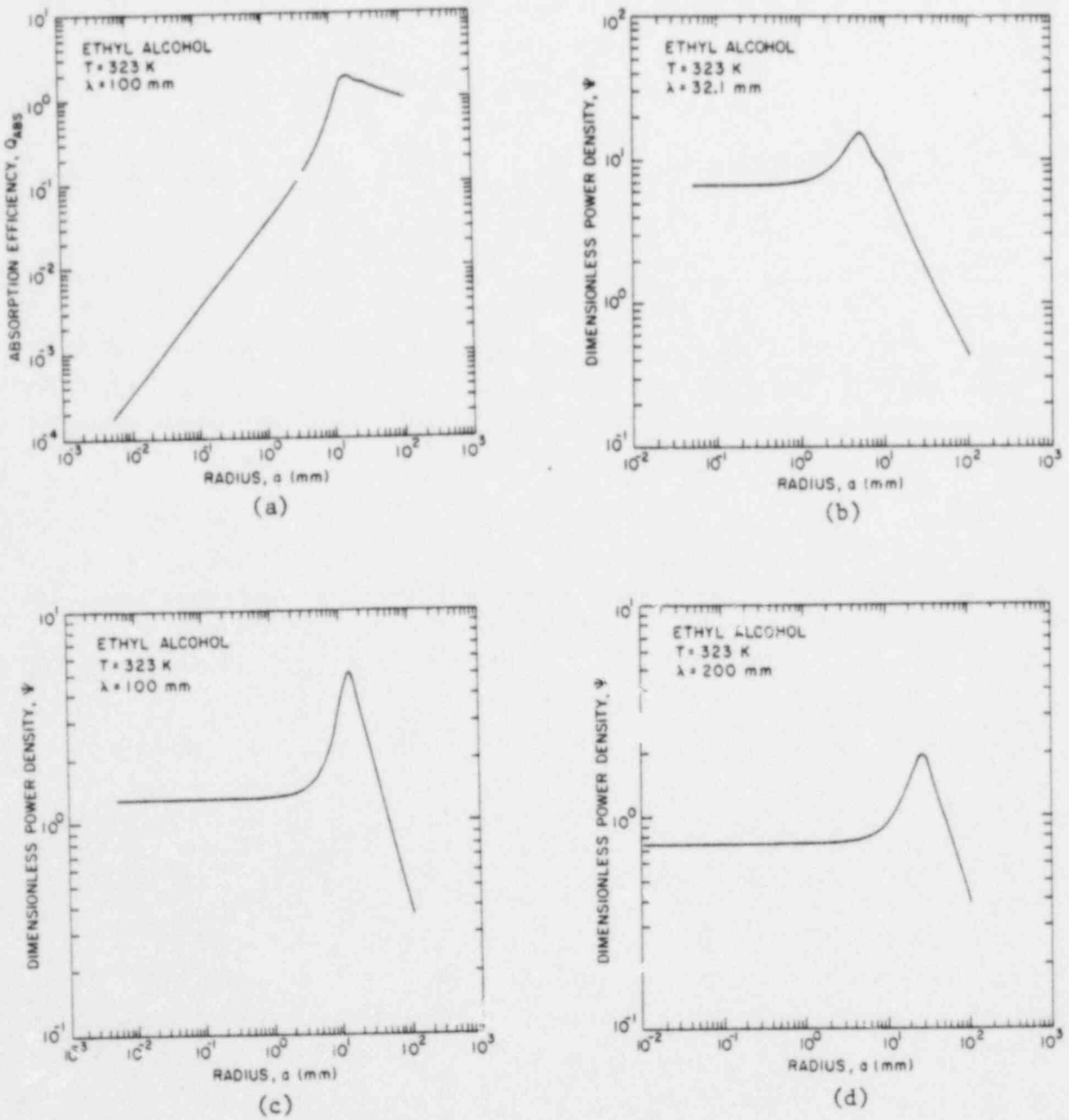

Figure 3.14 Absorption Characteristics of Ethyl Alcohol Spheres at T = 323 K: (a) Efficiency for λ = 100 mm; Power Density for (b) λ = 32.1 mm, (c) 100 mm, (d) 200 mm.
(BNL Neg. No. 12-581-80; 12-592-80; 12-587-80; 12-585-80)

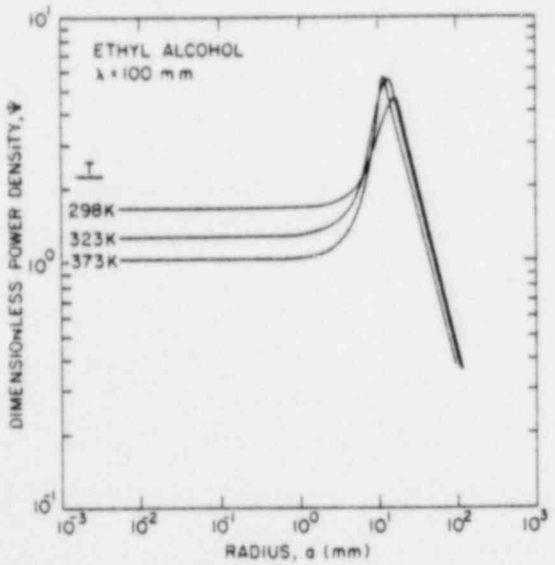

Figure 3.15 Power Density for Ethyl Alcohol and λ = 100 mm: T = 298 K, 323 K, 373 K.
(BNL Neg. No. 12-588-80)

imaginary indices of refraction which would: (i) extend the range of linearity of Q_{ABS} to centimeter-scale radii and (ii) smooth out the resonance region. Previous work suggested that lowering the real part of m^* tends to smooth out the resonances.

Figure 3.16 presents results of these DILISCA calculations for a radiation wavelength of 100 mm. The indices of refraction shown in Figure 16a extend the linear regime of Q_{ABS} to droplets of centimeter radius. The power density distributions shown in Figure 3.16b indicate that variations of less than a factor of two are possible with the m^* shown over a range of radius from 10^{-3} mm to 50 mm.

The parametric calculations presented in this section were not conceived with identification of a real material which would provide the droplet heating uniformity displayed in Figure 3.16b. Identification of such a liquid is the subject of the next section.

3.2.6 Mixtures of Polar and Non-Polar Molecules: Cyclohexane-Ethanol Solutions.

Westphal (1978) suggested that mixtures of polar and non-polar liquids could be tailored to provide continuously variable dielectric properties in the range presented in Figure 3.16. Combinations of the polar liquid ethyl alcohol with the non-polar liquid cyclohexane were investigated. The dielectric property data for mixtures of ethanol and cyclohexane were obtained from the work of Segal (1961). The data are presented in Figure 3.17 along with the extrapolation required to carry out the DILISCA calculations.

Calculations were performed for a range of ethanol-cyclohexane mixture compositions and temperatures. The wavelength was fixed at λ = 100 mm. Table 3.3 presents the complex indices of refraction computed from the data of Figure 3.17.

3.2.6.1 Effects of Mixture Composition.

The effect of mixture composition on the power density distribution of

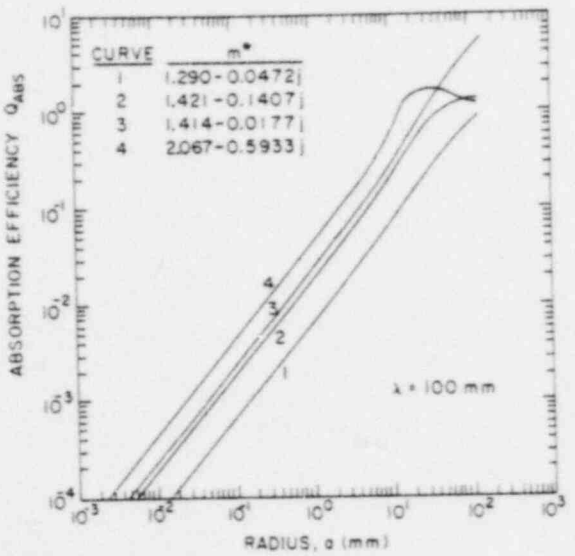

(a)

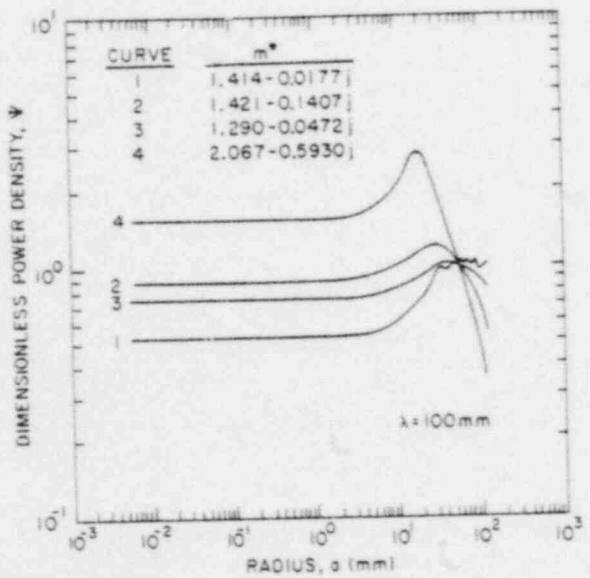

(b)

Figure 3.16 Absorption Efficiency (a) and Power Density (b) of Spheres with Variable Dielectric Properties for λ = 100 mm. (BNL Neg. No. 12-820-80; 12-819-80

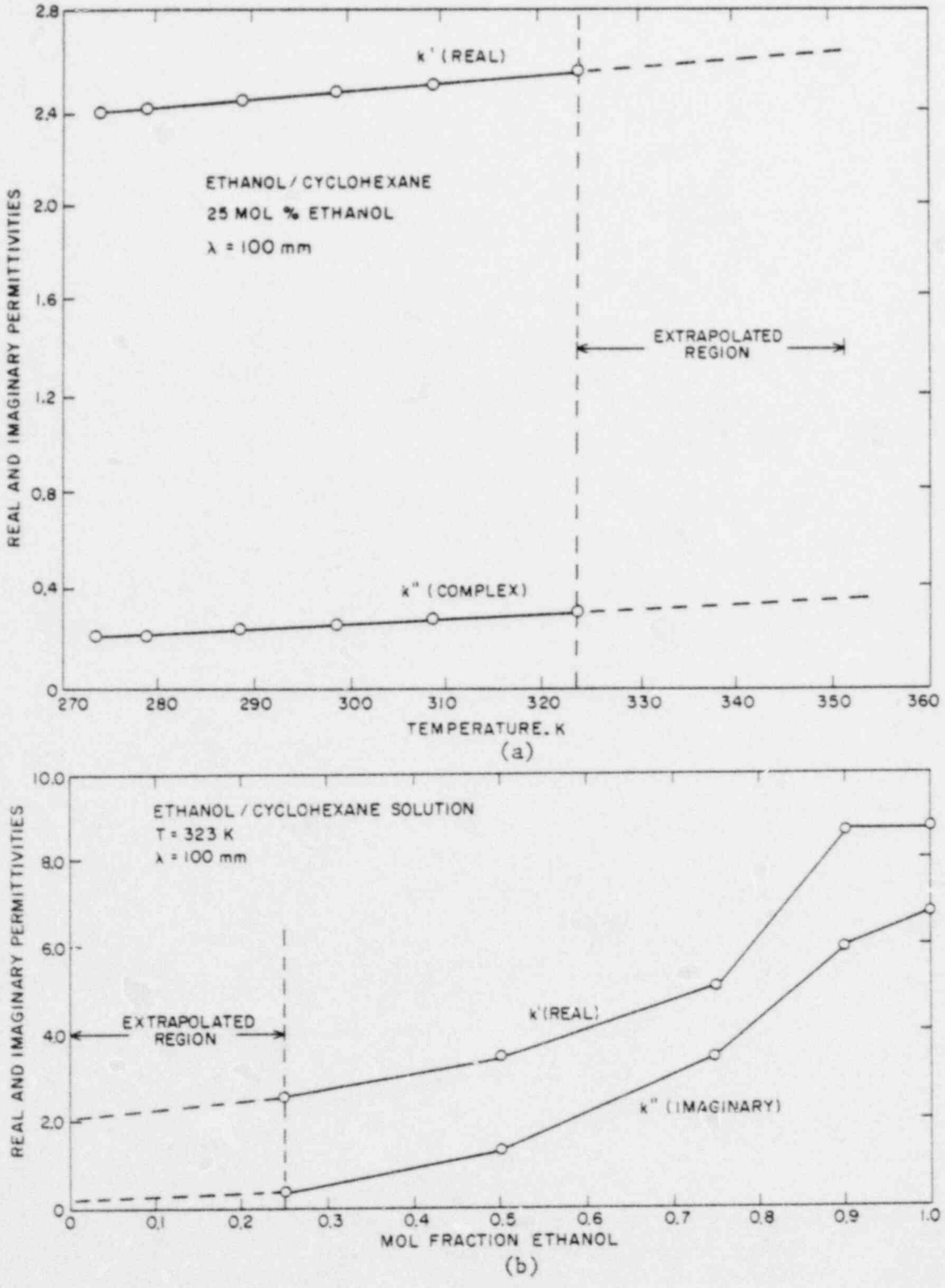

Figure 3.17 Dielectric Properties of Ethanol-Cyclohexane Solutions for λ = 100 mm: (a) 25 mol% Ethanol, Function of Temperature; (b) T = 323 K, Function of Ethanol Mol Fraction. (BNL Neg. No. 12-805-80; 12-603-80)

Table 3.3 - INDICES OF REFRACTION USED IN

CALCULATIONS: CYCLOHEXANE-ETHANOL. λ = 100 mm

T(K) mol fraction Ethanol	298	323	348
0.75	2.07 - 0.59j	2.36 - 0.73j	
0.50	1.756 - 0.29j	1.89 - 0.36j	
0.25	1.57 - 0.09j	1.61 - 0.10j	1.63 - 0.11j
0.12		1.49 - .05 j	

cyclohexane-ethanol droplets is shown in Figure 3.18. It is observed that these mixtures provide reasonably uniform power density distributions. The linear regime of Q_{ABS} is extended into the centimeter radius domain for the case of the low mol fraction ethanol mixtures. Figure 3.18 suggests that 12 -25 mol percent mixtures of ethanol provides uniform heating of liquid droplets over the range of radius up to approximately 50 mm. Over this range of droplet radius, the power density for 12 - 25 mol percent ethanol solutions varies by roughly a factor of two.

3.2.6.2 Effect of Temperature.

Calculations were performed over the temperature range 298 - 348 K. The results, not shown here, indicate that the effect of temperature is not significant for cyclohexane-ethanol mixtures.

3.2.6.3 Summary of Cyclohexane-Ethanol Solution Results.

Low mol fraction ethanol mixtures of ethanol-cyclohexane lead to droplet power density distributions which are uniform within a factor of two over the range of droplet radius of interest. Effects of temperature are negligible.

3.2.7 Summary of DILISCA Calculations.

The behavior of the energy absorption efficiency, Q_{ABS}, and the power density distribution, ψ, were evaluated as functions of droplet radius for various combinations of wavelengths and materials. The computer code DILISCA, representing a solution to Maxwell's equations in spherical geometry, was used in the study.

Water was investigated over a range of microwave wavelengths and temperatures. Figures 3.19 and 3.20 presents the results for Q_{ABS} and the dimensionless power density, ψ. The results indicate that water exhibits a strong dependence of power density on liquid geometry. The power density of water droplets of diameters less than 5 mm is two orders-of-magnitude lower than for centimeter-scale droplets exposed to the same incident energy flux. In a water system, therefore, uniform heating independent of liquid geometry cannot be achieved in the range of interest.

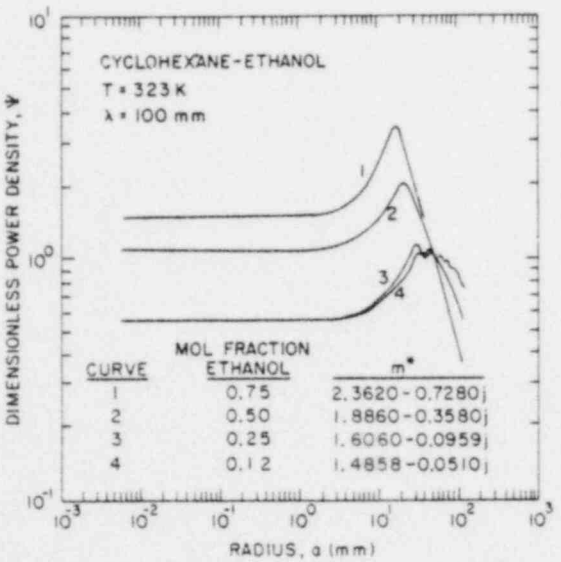

Figure 3.18 Power Density for Cyclohexane-Ethanol Spheres. (BNL Neg. No. 12-824-80)

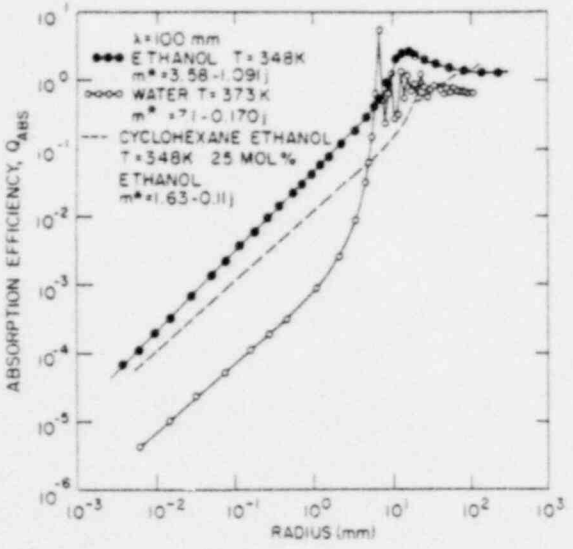

Figure 3.19 Absorption Efficiency for Pure Ethanol and for 25 mol% Ethanol Spheres Compared with Water Spheres. (BNL Neg. No. 12-821-80)

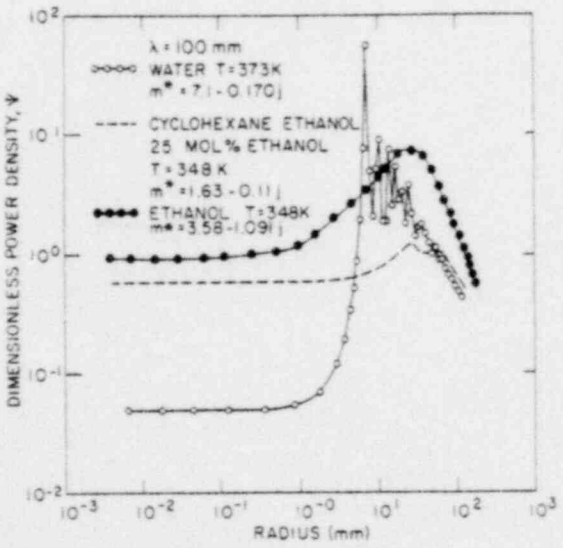

Figure 3.20 Power Density for Pure Ethanol and for 25 mol% Ethanol Spheres Compared with Water Spheres. (BNL Neg. No. 12-823-80)

A search for an alternative fluid system was performed. It was found that the dielectric properties of mixtures of polar ethanol and nonpolar cyclohexane could be tailored to optimize uniform volume-heating conditions. Results for a 25 mol% ethanol solution are presented in Figures 3.19 and 3.20. The power density of the ethanol-cyclohexane solution varies by only a factor of two over a range of droplet radius 10^{-3} to 50 mm.

3.3 Slab Geometry

3.3.1 Results for Water: Single Frequency Sources.

The results for power density distribution in slab geometry are presented in Figures 3.21 - 3.25. Figure 2.2 defines the geometry. In all cases, Region 2 represents the dielectric slab medium and Regions 1 and 3 refer to the bounding air regions (air was considered as free space). While Region 2 is of major interest here, and the results focus on the field distribution within the dielectric slab, some results are also shown for the field in the bounding air regions.

Figure 3.21 presents the normalized time-averaged electric-field (squared) for a 100 mm slab of water irradiated on a single side (Figure 21a) and bilaterally irradiated (Figure 3.21b) by 300 mm wavelength microwaves. The quantity $\overline{E^2}$ within this dielectric is proportional to the power density. The bilateral results assume that the frequency of the two sources are identical. A standing wave pattern is generated within the slabs for both single-sided and bilateral irradiation. The field within the slab is of low magnitude in both cases due to the poor coupling of the incident microwaves to the slab. The relatively large real part of the index of refraction for water leads to a large reflected energy flux in both cases. The pattern of standing waves is shown more clearly in Figures 3.22a and 3.22b, which are expanded versions of Figures 3.21a and 3.21b. In the case of single-sided irradiation, the standing wave pattern results from interference of the internally reflected wave with the transmitted wave. If internal reflection were to be neglected in the calculation their interference would be eliminated. The variation in power density would be caused only by exponential attenuation of the wave across the dielectric. This calculation is shown in Figure 3.22a.

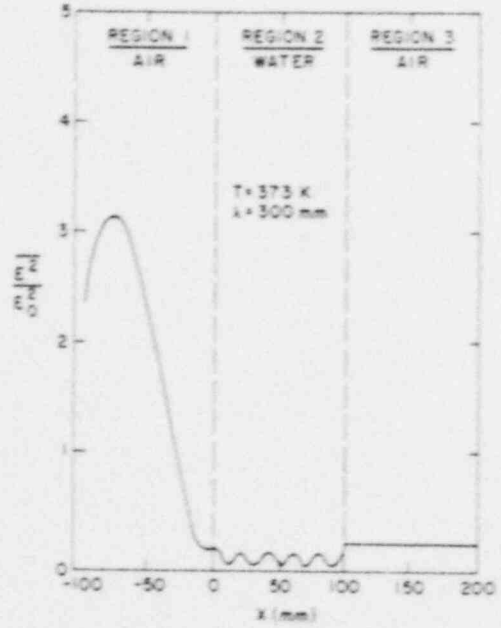

Figure 3.21 Electric Field Distribution in 100 mm Water Slab with Single-Sided (a) and Bilateral (b) Incident Radiation: λ = 300 mm. (BNL Neg. No. 12-832-80; 12-833-80)

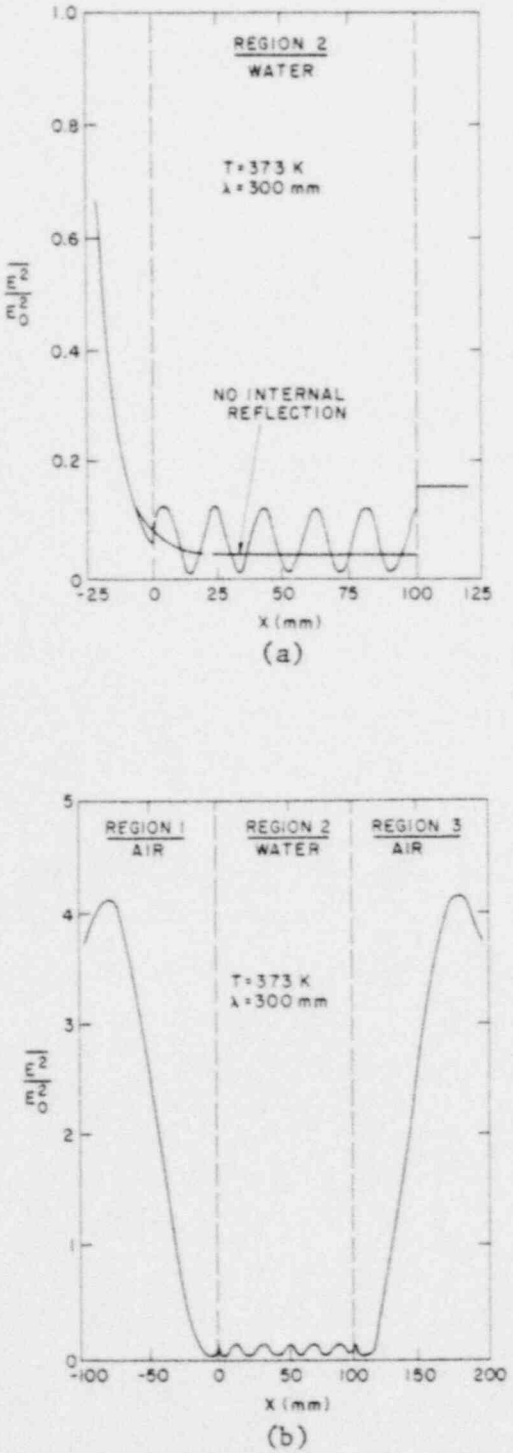

Figure 3.22 Electric Field Distribution in 100 mm Water Slab with Single-Sided (a) and Bilateral (b) Incident Radiation: Expanded Scale: λ = 300 mm. (BNL Neg. No. 12-829-80; 12-831-80)

Results for a wavelength of 100 mm are presented in Figure 3.23, shown on an expanded scale. The results again show standing wave patterns through the slabs. Figure 3.23a clearly shows the attenuation superimposed on the standing wave.

3.3.2 Results for Cyclohexane-Ethanol: Single Frequency Sources.

Results for irradiation of 100 mm slabs of 12 mol% ethanol solutions of cyclohexane-ethanol are shown in Figure 3.24 for λ = 300 mm. The smaller index of refraction (real part) for cyclohexane-ethanol leads to better penetration of the incident wave, and the field strength in the slab is increased. Standing waves are observed in both single-sided and bilateral irradiation. The wavelength of the standing wave is smaller for cyclohexane-ethanol. Figure 3.24a shows the results for the calculation which does not account for internal reflection. The standing waves do not appear and exponential attenuation results.

Results for irradiation by 100 mm wavelength microwaves are shown in Figure 3.25. The results are similar to the case of λ = 300 mm, but the wavelength of the standing wave is larger.

In both the λ = 100 mm and λ = 300 mm results presented above it is apparent that large amplitude standing waves develop in the slab for bilateral irradiation. This is attributed to interference of the transmitted waves, which are of identical frequency.

3.3.3 Results for Bilateral Slab Irradiation with Sources of Slightly Different Frequency.

The results presented in Section 3.3.1 and 3.3.2 show that standing waves develop in slabs irradiated bilaterally with microwave sources of identical frequency. This can be attributed primarily to interference of the waves which are transmitted into the slabs. The analysis, presented in Section 2.3, of the problem of bilateral irradiation of a slab with sources of slightly different frequency leads to the conclusion that these standing waves do not develop as a result of interference of the transmitted waves. If, in addition, internal reflection is neglected, then the variation in power density across the slab is shown to be

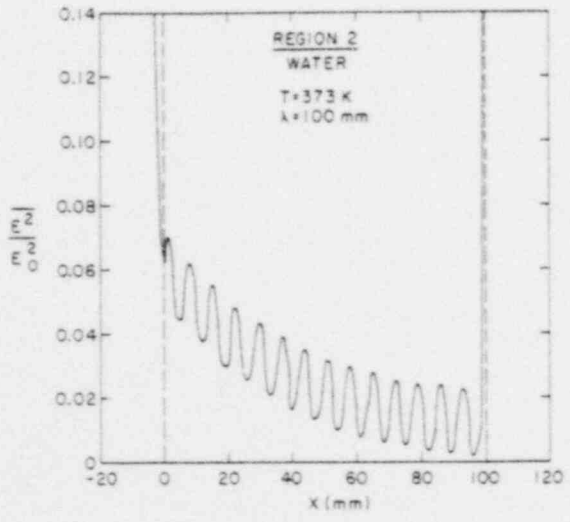

(a)

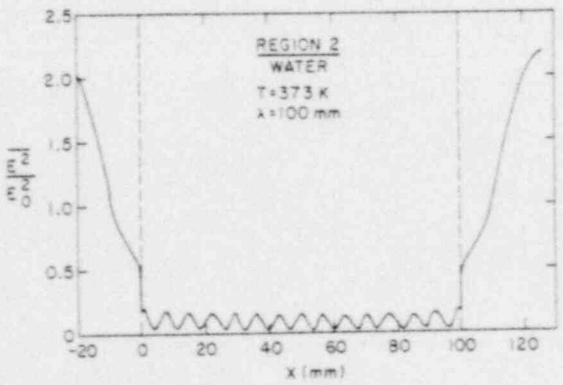

(b)

Figure 3.23 Electric Field Distribution in 100 mm Water Slab with Single-Sided (a) and Bilateral (b) Incident Radiation: λ = 100 mm. (BNL Neg. No. 12-825-80; 12-826-80)

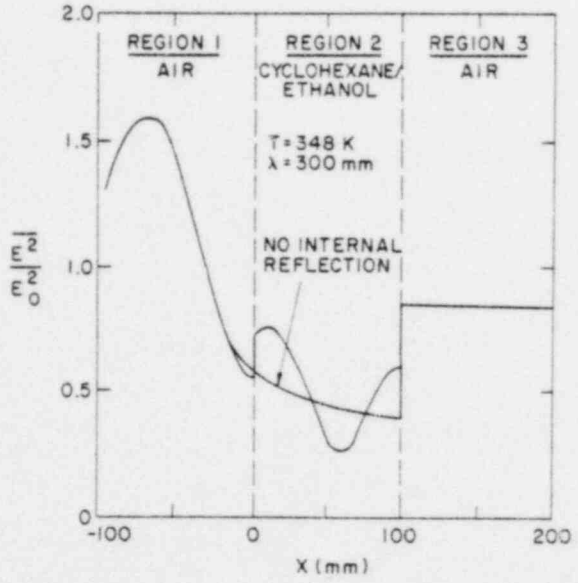

(a)

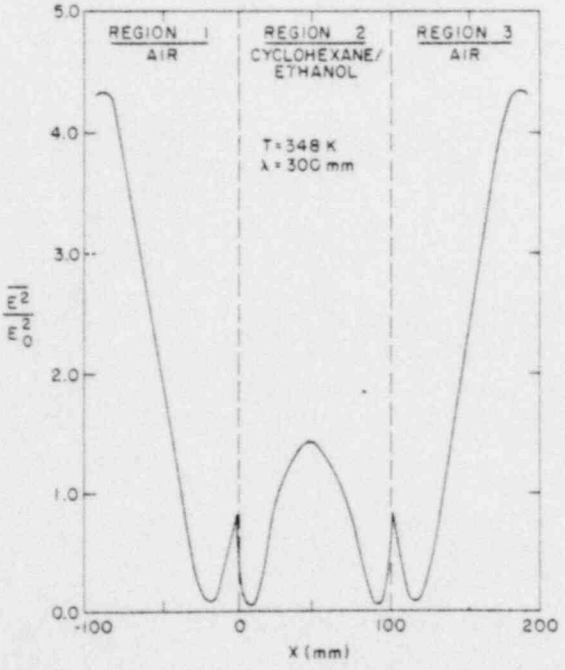

(b)

Figure 3.24 Electric Field Distribution in 100 mm Cyclohexane-Ethanol Slab with Single-Sided (a) and Bilateral (b) Incident Radiation: λ = 300 mm.
(BNL Neg. No. 12-827-80; 12-828-80)

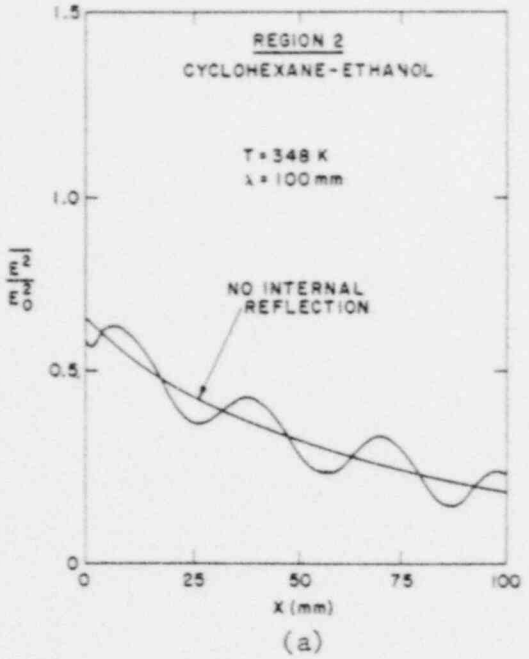

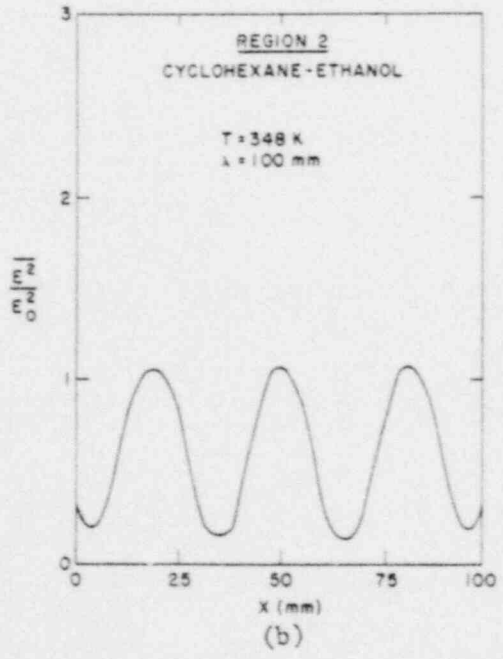

Figure 3.25 Electric Field Distribution in 100 mm Cyclohexane-Ethanol Slab with Single-Sided (a) and Bilateral (b) Incident Radiation: λ = 100 mm. (BNL Neg. No. 12-830-80; 12-834-80)

$$\frac{P(x)}{P_o} = \cosh(2\alpha x) \qquad (3.1)$$

for $-\ell/2 < x < +\ell/2$. This expression can be shown to be equivalent to the sum of two decaying exponentials, which represents the attenuation of two waves of equal source strength transmitted into the slab from opposite directions.

The power density distribution given by Equation (3.1) was used to compute the ratio of the maximum power density (which occurs at $x = \pm \ell/2$) to the minimum power density (which occurs at $x = 0$).

Figure 3.26 presents the maximum to minimum power density ratio for irradiation of both water and cyclohexane-ethanol with microwaves of wavelengths λ = 100 mm and λ = 300 mm. A range of slab thicknesses up to 300 mm is considered. Both materials are considered to be at their normal boiling points. The results indicate that the attenuation of power density across a slab due to dielectric losses is quite significant for water. The attenuation is, however, significantly smaller for cyclohexane-ethanol.

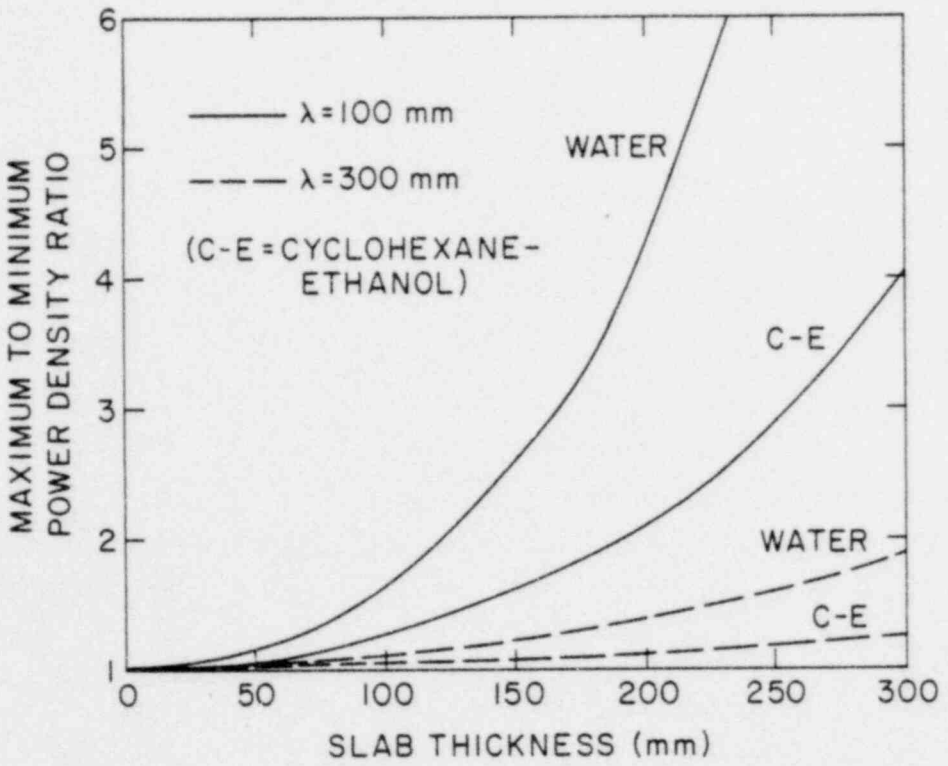

Figure 3.26 Maximum-to-Minimum Power Density Ratios for Water and Cyclohexane-Ethanol Slabs with No Internal Reflections: λ = 100 and 300 mm. (BNL Neg. No. 12-813-80)

IV. HEATING UNIFORMITY EXPERIMENTS

4.1 Introduction.

The theoretical analyses presented in Chapter III suggest that (i) the heating rate of liquid dielectrics which are exposed to microwave radiation is strongly affected by liquid geometry and dielectric properties and (ii) strong spatial power density gradients may develop upon irradiation of dielectrics with microwaves. The analyses were performed for simple geometries and simple source configurations. Two series of experiments were carried out in a microwave oven in order to evaluate the basic concepts and to determine whether similar behavior is to be expected in a more complex radiation environment than assumed in the analysis.

The first set of experiments addressed the effect of liquid geometry on power density. These experiments are described in Section 4.2. In the second set of experiments the spatial distribution of power density in an object irradiated in an oven was investigated. This study is described in Section 4.3.

4.2 Effect of Liquid Geometry on Power Density.

4.2.1 Experiment Description.

An experiment was conducted to measure the effect of geometry on the power density of liquid samples exposed to microwaves in a microwave oven configuration. The oven used in the experiment is a LITTON Model 419 oven, rated at 600 W, and operates at a standard microwave frequency of 2450 MHz. The power output of this particular oven is controllable only through "duty-cycling", i.e., the microwave source is periodically turned on and off in order to provide a time-average power output. In the experiments described below this method was not used. All measurements were made at full power conditions.

The objective of the experiments was to measure the power density of cylindrical samples of liquid of 10 mm diameter and of variable height, relative to the power density of a fixed geometry volume of liquid. The microwave oven cavity is shown in Figure 4.1 along with two liquid containers. The large container was a thin-walled Pyrex glass beaker of 100 mm diameter. The test liquid was filled to a height of 95 mm in most of the experiments. The second container is

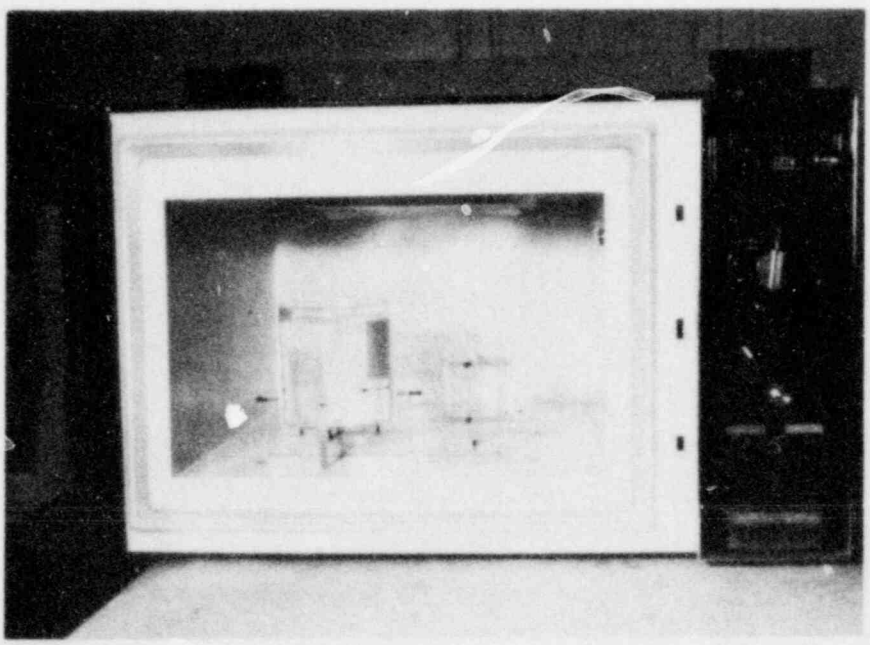

Figure 4.1 Photograph of Microwave Oven and Sample Test Containers. (BNL Neg. No. 12-606-80)

a 10 mm diameter Pyrex cylinder with a flat bottom. This container was filled with test liquid to a height H, which is the primary experimental parameter.

An experiment was carried out by first filling the reference beaker with a fixed volume of liquid and filling the cylindrical tube to a selected height H. The initial liquid levels and temperatures were recorded. The samples were inserted into the oven and the power turned on. The liquid samples were irradiated for a predetermined time interval. After the power was turned off, the samples were mixed and a final temperature for each of the two containers were recorded. All temperatures were measured with a 1.59 mm (1/16-in) diameter stainless-steel sheated, chromel-alumel, grounded-junction thermocouple.

The power densities of the reference and variable-height containers were computed by using an energy balance on the liquid containers together with the measured temperatures and liquid masses. It is assumed that all of the microwave energy is deposited in the liquid and that a negligible fraction is deposited in the glass. It is also assumed that glass and the water are at the same temperature. A lumped-parameter energy balance on one of the test containers is

$$Q''' \frac{m_\ell}{\rho_\ell} = \left(m_\ell c_\ell + m_g c_g \right) \frac{\Delta T}{\Delta t} \tag{4.1}$$

or

$$Q''' = \left(1 + \frac{c_g m_g}{c_\ell m_\ell} \right) \rho_\ell c_\ell \frac{\Delta T}{\Delta t} \tag{4.2}$$

The ratio of the power density of the variable height liquid, Q'''_H, to that of the reference container liquid, Q'''_{REF} is, then,

$$\frac{Q'''_H}{Q'''_{REF}} = \frac{\left[\left(1 + \frac{c_g m_g}{c_\ell m_\ell} \right) \frac{\Delta T}{\Delta t} \right]_H}{\left[\left(1 + \frac{c_g m_g}{c_\ell m_\ell} \right) \frac{\Delta T}{\Delta t} \right]_{REF}} \tag{4.3}$$

The dimensionless power density given by Equation (4.3) was computed from the temperature data as a function of H, where H was varied from 1 mm to 95 mm. The distribution of power density (as a function of H) was determined for two test fluids: water and a mixture of cyclohexane and ethyl alcohol of composition 12 mol % ethyl alcohol.

Samples were irradiated for 30s time intervals. In this time period the temperature rise of the reference container liquid was approximately 6 K. The cylindrical container temperature varied from approximately 3 K for small H, up to approximately 60 K for the larger H samples (see Section 4.3 below). Assuming an error of $\pm$ 1 K in the temperature measurements, it is estimated that the error in the computed power density is as much as $\pm$ 50 % for H of millimeters and $\pm$ 20-25 % for H in the centimeter range.

In addition to the source of random error discussed above, an additional systematic error was probably encountered for small H, although its magnitude was not evaluated. For small depths H of liquid in the 10 mm diameter glass cylinder the heat capacity of the thermocouple in contact with the liquid approaches that of the water. Under these conditions the thermocouple, inserted from initially room temperature into the warm liquid, can reduce the liquid temperature as it comes into thermal equilibrium with the thermocouple. This means that the computed power density ratio may be artificially low for the smallest values of H. The magnitude of this effect, however, is computed to be on the order of 10-15 %.

4.2.2 Experimental Results.

The results of the experiment discussed above are presented in Figure 4.2. Results are shown for water and for the cyclohexane-ethanol solution. The results clearly demonstrate a very strong dependence of the power density on liquid geometry. Order-of-magnitude variations are observed for water. An absorption resonance is observed at approximately H = 40-50 mm. The water temperature rise at the resonance exhibited a large degree of scatter, but ranged in magnitude up to approximately 60 K. This is clearly greater than the temperature rise of approximately 6 K characteristic of the liquid in the reference container.

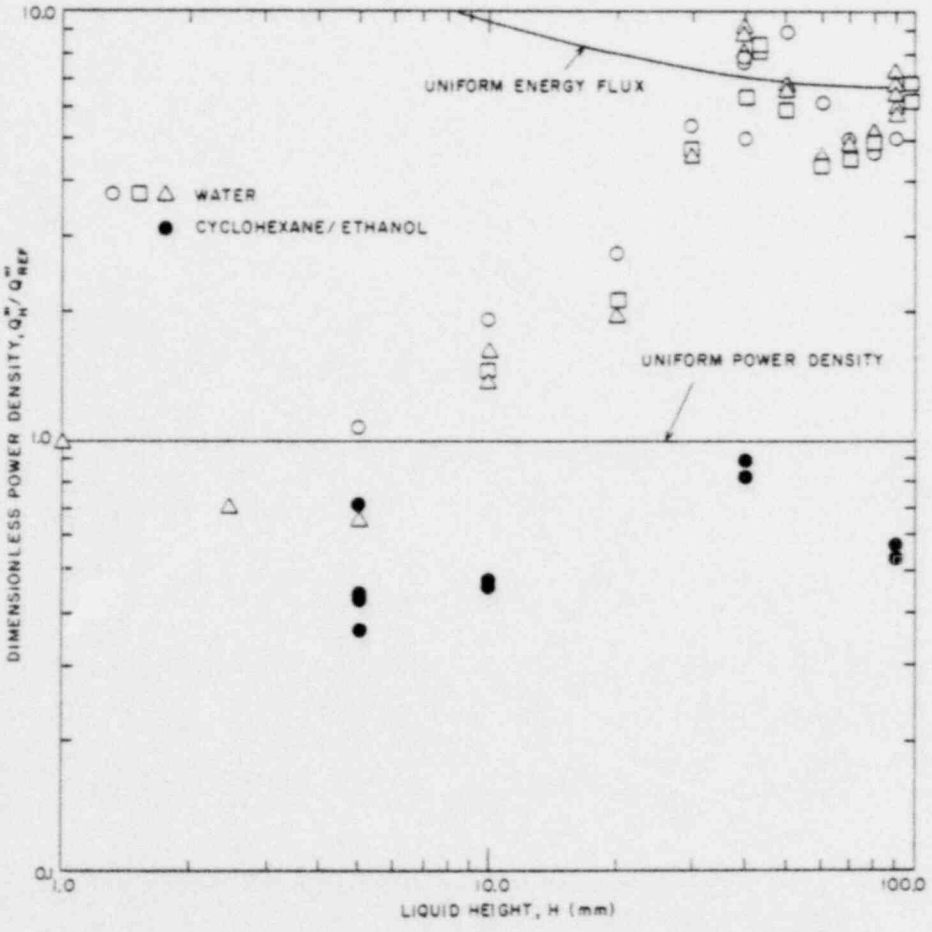

Figure 4.2 Dimensionless Power Density of Liquid Samples vs. Liquid Height. (BNL Neg. No. 12-810-80)

The data taken using ethanol-cyclohexane are not as extensive as for water. The results are distinctly different than for water. In general the power density of the 10 mm cylindrical diameter samples are less than for the reference liquid container. The variation in power density is much smaller than for the case of water.

A comparison of the water data with the cyclohexane-ethanol data suggests that the effect of liquid geometry is considerably weaker for the organic solution compared with water.

Also shown in Figure 4.2 are power density ratios computed on the basis of two simplified models. The first is based upon the assumption that the power density is independent of geometry. This is represented by the "uniform power density" curve. This model effectively implies that the temperature rise of the samples exposed simultaneously in the microwave oven are identical, independent of geometry. This assumption, as shown in Figure 4.2, is clearly inaccurate. An effect of liquid geometry is apparent which is not characterized by the simple "uniform power density" assumption. It should be noted, however, that the cyclohexane-ethanol data is more closely characterized by this assumption than is water.

A second model of energy absorption in a microwave oven is based upon two assumptions: (i) the rate of energy absorbed is proportional to the surface area of the sample and (ii) the incident energy flux is uniform across the surface of the samples under irradiation. Under these assumptions, the power density of the reference liquid is

$$Q'''_{REF} = \phi_{INC} \frac{A_{s,REF}}{V_{REF}} \tag{4.4}$$

and for the liquid in the 10-mm cylinder

$$Q'''_{H} = \phi_{INC} \frac{A_{s,H}}{V_{H}} \tag{4.5}$$

The power density ratio is

$$\frac{Q'''_H}{Q'''_{REF}} = \frac{A_{s,REF}}{V_{REF}} \cdot \frac{V_H}{A_{s,H}} \tag{4.6}$$

where

$$V_H = \pi D^2 H \tag{4.7}$$

$$A_{s,H} = 2(\pi D^2) + \pi D H \tag{4.8}$$

and $D = 10$ mm. The quantity $A_{s,REF}/V_{REF}$ is a constant for the reference container.

Equation (4.6) is plotted in Figure 4.2 as the "uniform energy flux" model. This model also clearly does not adequately characterize the data. Except for the case of water, for $H > 30$ mm, the assumption clearly overestimates the power density of the 10 mm diameter samples compared with the reference container sample.

4.2.3 Summary.

The experimental results described above suggest:

(i) The power density of multiple water samples exposed in a microwave oven is a strong function of sample geometry.

(ii) The power density of multiple samples of cyclohexane-ethanol solutions (12 mol percent ethanol) exposed in a microwave oven is much less dependent on sample geometry than is water.

(iii) The power density of samples of liquid irradiated in a microwave oven is not adequately characterized by either the assumption of uniform power density or the assumption of uniform incident energy flux.

These findings qualitatively support the analytical results of Section 3.2, albeit for a different geometry and for a different irradiation environment.

4.3 Spatial Distribution of Power Density.

4.3.1 Experiment Description.

An experiment was carried out to measure the spatial variation of power density in a sample of liquid exposed in a microwave oven. A container of liquid was inserted into an oven and irradiated for a fixed period of time. The sample was subsequently quickly removed and a thermocouple rake was inserted into the liquid. The temperatures at several locations in the liquid were measured simultaneously. The power densities at these locations were calculated from the temperature rise of the liquid. It was assumed that heat losses and liquid motion in the test container were negligible. The power density is given by

$$Q''' = \rho_\ell c_\ell \frac{\Delta T}{\Delta t} \tag{4.9}$$

where ΔT is the recorded temperature rise for an irradiation period of Δt.

Figure 4.3 shows the microwave oven, together with the test container, a thin-walled glass beaker, and the thermocouple rake and support rig. Six chromel-alumel, steel-sheated, grounded junction thermocouples were used. They are shown in Figure 4.3 in a staggered array. Most of the experiments, however, were carried out with the thermocouples at the same elevation. The glass beaker was 100 mm in diameter and 100 mm long. It was filled with liquid to a height of 90 mm. Water was used exclusively in this experiment.

An experiment was performed by first filling the beaker with water. The water was irradiated for 30 seconds and was subsequently removed from the oven and placed on the support rig. The thermocouple rake was positioned at the desired location. Temperatures at the six radial locations for a fixed distance below the free surface were recorded. This procedure was repeated for various levels below the free surface.

4.3.2 Experimental Results.

The experimental data showed variations of temperature with radial position of, generally, less than 0.5 K. As a result, the radial variation of temperature rise is not considered here. Figure 4.4 presents the measured temperature

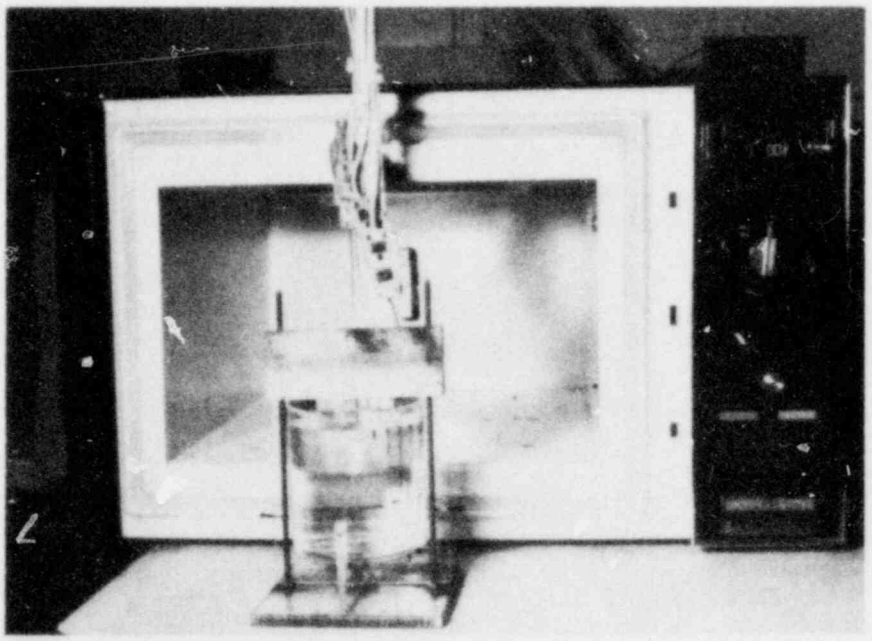

Figure 4.3 Photograph of Oven, Test Container and Temperature Rake Used in Power Density Experiments. (BNL Neg. No. 12-609-80)

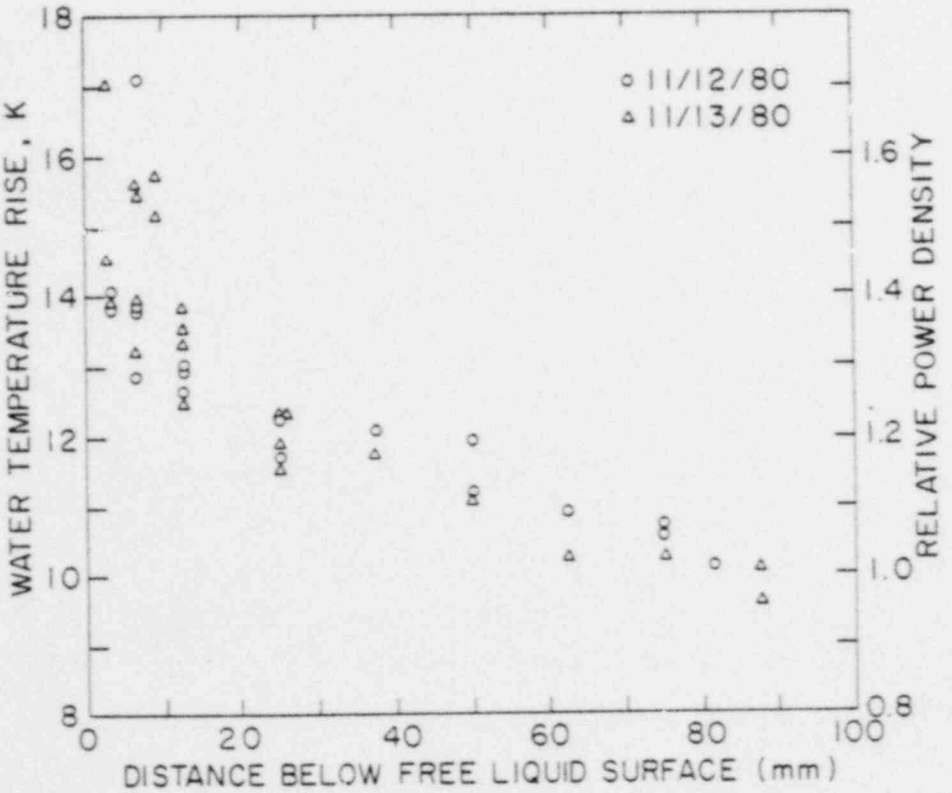

Figure 4.4 Measured Spatial Variation of Power Density in Test Container. (BNL Neg. No. 12-817-80)

rise of the liquid as a function of depth below the free surface. This temperature rise is proportional to the local power density, and is also represented as such in Figure 4.4. The measured temperature rise varies from approximately 10 K at the bottom of the beaker to approximately 14-18 K near the free surface. A sharp temperature gradient is observed in the vicinity of the free surface, and much exeperimental scatter is also observed. The scatter is attributed to the relatively imprecise positioning of the thermocouple rake in the liquid.

The power density in the liquid varies by 60% across the height of liquid in the test container. This variation is probably due to the design of the oven, in which the microwave energy is ducted into the cavity through the top surface of the oven. The free surface of the test liquid is directly below the porthole which supplies the microwave energy flux.

4.3.3 Summary.

The results of the experiment support the conclusion that power density gradients are to be expected in liquids exposed to microwave radiation. Water contained in a cylindrical container and exposed in a microwave oven showed power density variations of 60% in the vertical direction, and little measureable variation in the radial direction. The observed variation may be attributable to microwave cavity design. The magnitude of the variation cannot be extrapolated to other microwave oven designs.

V. IMPLICATIONS AND CONCEPTUAL DESIGN OF MICROWAVE BOILING EXPERIMENT

5.1 Introduction.

The work presented in the previous four chapters of this report was directed towards the evaluation of microwave dielectric heating as a simulation of the nuclear heat source in conjunction with LMFBR transition phase boiling simulation experiments. Two fundamental issues were defined in Chapter I with respect to the adequacy of the microwave heating technique: (i) liquid power density uniformity and (ii) predictability of the liquid power density distribution. Ideally, the liquid power density in the two-phase boiling flow conditions under microwave irradiation would be uniform. If this cannot be achieved, then the power density distribution should be predictable. This chapter discusses the implications of the material presented in the prior chapters of this report from the point of view of these two issues. Thus, the adequacy of microwave dielectric heating for the present application is evaluated. This evaluation is presented in Section 5.2. A conceptual design of a microwave boiling experiment is presented in Section 5.3 which derives from the totality of the work performed in this study.

5.2 On the Adequacy of Microwave Dielectric Heating for Transition Phase Boiling Studies.

The two-phase boiling configuration under conditions of microwave heating is expected to be characterized by a spectrum of liquid-vapor geometric structures. Single-phase liquid structures of order centimeters in dimension, spherical bubbles dispersed in a continuous liquid phase, irregular liquid filaments of millimeter or centimeter scale surrounded by vapor, and liquid droplets of millimeter (or less) size dispersed in vapor, all may simultaneously exist in a single microwave environment. The analytical tools necessary for computation of the power density distribution under these conditions do not exist. Consequently, two distinct problems were studied in prior chapters, with the objective of providing estimates of the extent of power density variation under boiling conditions. These are: (i) analysis of the power density distribution of liquid droplets exposed to the same incident microwave radiation field, and (ii) analysis of the power density distribution across slabs of

roughly 100 mm in width, exposed to either single sided or bilateral, normally incident microwave radiation.

5.2.1 Droplet Power Density Problem: Implications.

The analysis of the droplet power density problem provides us with estimates of the relative heating rates of liquid masses of a spectrum of dimensions if they are exposed to the same source of radiation. The results of the analysis, presented in Section 3.2, demonstrates that the power density of water droplets is extremely sensitive to droplet dimensions. Millimeter droplets are characterized by power densities which are approximately 2 orders-of-magnitude lower than centimeter-size droplets. This conclusion is supported by the experiments performed in a microwave oven, described in Chapter IV, albeit for a different geometry. The data show an order-of-magnitude variation in the power density of cylindrical water samples of constant diameter but variable height. The power density of millimeter-height samples were a factor of 10 less than for centimeter-high samples.

The results summarized above are interpreted to imply that if a microwave boiling experiment lends to conditions in which water droplets coexist with continuous masses of centimeter scale, then the microwave energy would be effectively uncoupled from the droplets of millimeter diameter scale and would, instead, be absorbed in the larger available liquid volumes. This situation argues against the use of microwave heating with water as the test fluid in the boiling experiments, since the major reason for using this heating method is to enable dispersed droplets to remain coupled to the energy source.

Parametric studies showed that the power density distribution for liquid droplets with complex index of refraction (real part) less than that of water would be more uniform. Cyclohexane-ethanol solutions were found to have indices of refraction that lead to uniform power densities up to the centimeter-diameter range (i.e., the Raleigh scattering regime is extended to larger radii). The uniformity of droplet heating was found to be acceptable for 12-25 mol% ethanol solutions of cyclohexane-ethanol. The experiments described in Chapter IV, though limited in number for cyclohexane-ethanol solutions, support the conclusion that the power density distribution is considerably more uniform for these solutions than for water.

These results suggest that a cyclohexane-ethanol mixture of 12-25 mol% ethanol is a candidate fluid system for use with microwave dielectric heating, from the standpoint of uniformity of droplet heating. It is expected that, on the basis of the foregoing, that cyclohexane-ethanol droplets would heat as effectively as larger liquid volumes and would remain coupled to the microwave energy source in the presence of larger liquid volumes.

5.2.2 Spatial Distribution of Power Density: Implications.

The literature review presented in Chapter I suggests that strong spatial variations in power density are to be expected upon microwave irradiation of materials with dielectric properties similar to water. This conclusion is supported by both analytical and experimental results and applies to homogeneous materials of various geometries.

The spatial distribution of power density within an object under microwave irradiation can be calculated for free-space irradiation of relatively simple geometry systems. Little information is available for microwave oven irradiation, and analytical techniques for computing power density distributions under these irradiation conditions are unavailable.* It is not possible, therefore, to predict the effect of dielectric properties on the power density distribution of samples exposed to microwave irradiation in a microwave cavity (oven).

The slab irradiation problem was analyzed in order to provide an estimate of the spatial distribution of power density across the single-phase liquids of interest under microwave irradiation. This simplified calculation also provides a method of comparing the power density distributions of different index of refraction liquids, in order to determine whether the power density variations can be minimized by suitable choice of liquid properties.

The specific problems analyzed were those of single-sided and bilateral irradiation of slabs with normally incident radiation. It was assumed that the

---

* Analytical techniques used to compute electric field intensities in particle accelerator design may be applicable, but have not been used for microwave oven applications.

irradiation takes place in free space. This problem is highly idealized. Irradiation in either a microwave cavity (oven) or in a waveguide would lead to different distributions.

The slab calculation results presented in Section 3.3 show that power density variations across slabs are due to wave interference effects and due to energy flux attenuation as a result of power absorbed in the lossy dielectric. The wave interference effects are ascribable to interaction of transmitted and internally reflected waves, and to interaction of the two transmitted waves in the case of bilateral irradiation of identical frequency sources. The calculational results show that strong power density variations are found both for water and for cyclohexane-ethanol. The major difference in the behavior of the two materials is the wavelength of the standing wave that develops in the slab, and in the extent of attenuation in the material.

The results for bilateral irradiation of a slab with identical frequency sources indicate that transmitted wave interference results in large amplitude power density variations across the slab for both water and cyclohexane-ethanol.

Based upon the results described above, it is concluded that wave interference effects, together with the power density variations that result, cannot be avoided upon exposure of slabs to either single-sided irradiation, or with bilateral irradiation with identical frequency sources. The choice of fluids does not alter this basic conclusion.

The power density distribution within a multiphase fluid exposed in a microwave oven cannot be predicted. However, the results described above are interpreted qualitatively to apply to microwave oven irradiations as well as for the free-space slab irradiation discussed above; significant power density gradients cannot, therefore, be ruled out upon irradiation of fluids in a microwave oven, no matter what fluid properties are chosen. It is concluded that a microwave oven irradiation environment for the boiling simulation experiments is inappropriate for the following reasons:

(i) power density gradients in the test fluid are expected to exist and to be of significant magnitude.

(ii) the power density distributions cannot be predicted with available methods.

5.3 Conceptual Design of Microwave-Heated Boiling Experiment.

5.3.1 Background.

The analysis described in Section 3.3 suggests that if a slab is bilaterally irradiated with microwaves and if

(i) the two sources of radiation operate at slightly different frequency

(ii) internal reflections within the medium can be eliminated

then wave interference effects would be negligible. Under these conditions, standing waves would not develop. The resulting power density variations would be due only to attenuation of the transmitted waves across the absorbing dielectric.

If the conditions listed above are satisfied, then the power density distribution across the slab of width 'ℓ', is simply given by

$$\frac{P(x)}{P_o} = \cosh (2\alpha x) \qquad (5.1)$$

for $-\ell/2 < x < +\ell/2$, and

$$\alpha = \frac{2\pi}{\lambda} n' \qquad (5.2)$$

It has been shown in Section 2.4.3 that the power density variations across cyclohexane-ethanol slabs are less than 25% for slab widths of 300 mm or less.

A physical system can be designed to provide conditions which are similar to those described above. The concept described below was developed in conjunction with discussions held with the staff of the Raytheon Corporation. The basic ideas were proposed by Raytheon. Their feasibility, however, have yet to be demonstrated in a real laboratory experiment. The proposed physical system is as follows:

Consider a hollow, loss free rectangular waveguide, with sides of dimensions a and b. Assume that the waveguide is excited by a source of frequency f, corresponding to a wavelength in free space of λ. It has been

shown (e.g. Kraus, 1953) that the electric field within the waveguide is the sum of the fields of an infinite number of "modes". However, for a given guide geometry, there exists a cutoff frequency f_c below which a given mode cannot be propagated within that particular waveguide. The cutoff frequency is given by

$$f_c = \frac{1}{2\sqrt{\mu\epsilon}} \sqrt{\left(\frac{n}{a}\right)^2 + \left(\frac{m}{b}\right)^2} \tag{5.3}$$

which corresponds to a cutoff wavelength, λ_{co}, given by

$$\lambda_{co} = \frac{2}{\sqrt{\left(\frac{n}{a}\right)^2 + \left(\frac{m}{b}\right)^2}} \tag{5.4}$$

where m and n represent the integers which define the mode of excitation of the waveguide. The smallest mode numbers corresponding to a non-zero electric field are m = 1 and n = 0. For this mode the electric field is given by:

$$E_y = \frac{\gamma Z_{yz}}{k^2} H_o \frac{\pi}{b} \sin\frac{z}{b} e^{j(\omega t - \gamma x)} \tag{5.5}$$

where $\gamma = \sqrt{\left(\frac{\pi}{b}\right)^2 - \left(\frac{2\pi}{\lambda}\right)^2}$

$$k^2 = \left(\frac{\pi}{b}\right)^2$$

The cutoff wavelength for the m = 1, n = 0 mode is

$$\lambda_{co} = 2b.$$

If a < b, then a wavelength of 2b is the longest that can be propagated in the mode m = 1, n = 0. If the waveguide is excited with a frequency corresponding to λ = 2b, then the higher order modes will not propogate. For example, the cutoff wavelength for the mode m = 2, n = 0 is λ_{co} = b.

Therefore if the waveguide is excited with a frequency corresponding to λ = 2b, the mode m = 2, n = 0 will not propogate since this wavelength is greater

than the cutoff frequency $\lambda_{co} = b$. The waveguide will, therefore, operate as carrier of a single mode, with the electric field characterized by Equation (5.5).

The field represented by Equation (5.5) is a travelling wave which propogates propogates along the axis of the waveguide. Because the guide operates in a single mode, wave interference effects do not occur, and standing waves do not develop. The mean-square electric field, proportional to the electromagnetic energy density, is constant along the axis of the waveguide.

Assume now that the waveguide is filled with a homogeneous, lossy liquid dielectric. The liquid is contained by the walls of the waveguide and by a lower base plate. The discontinuity in dielectric properties presented by the base plate-liquid interface would result in partial reflection and transmission of the wave. A standing wave would then be generated in the guide. In order to avoid this behavior, assume that the base plate is designed to eliminate the reflected wave. This could be done, for example, with a 1/4-wavelength plate (Kraus, 1953). If the reflected wave could thus be suppressed, then the resulting energy density within the waveguide would be exponentially attenuated by dielectric losses. The power in the waveguide would be given by (Kraus, 1953)

$$\phi = \phi_o \ e^{-2\alpha x} \tag{5.6}$$

where α is the attenuation coefficient given by Equation (5.2). The power density would be proportional to the energy density and would be given by

$$P = P_o e^{-2\alpha x}$$

If it is assumed that sources of slightly different frequency were placed at each end of the waveguide, and if the reflected waves could be eliminated from both ends of the waveguide, then the waves propogating in opposite directions would not interfere. For sources of equal strength, the power density would be simply the sum of two decaying exponentials,

$$P = P_o \left\{ \exp\left[-2\alpha x\right] + \exp\left[-2\alpha(x-\ell)\right] \right\} \tag{5.7}$$

which is identical to Equation (5.1).

5.3.2 Design of Microwave Applicator for Boiling Experiments.

Based upon the above considerations it is proposed that the microwave boiling experiments be carried out in a microwave waveguide. The system is shown schematically in Figure 5.1. The dielectric liquid is contained in a low-loss glass container. The container would be surrounded by a metallic mesh sheath, which would function as the walls of the waveguide. The mesh can be designed to adequately shield the environment from microwave radiation and, at the same time, to permit visual observation of the boiling processes within the two-phase dielectric medium.

Microwave energy is directed into the waveguide from both ends, from two sources which operate at slightly different frequencies, as shown in Figure 5.1. "Bidirectional couplers" are used to permit energy to be transmitted into the waveguide from the source in one direction, and would allow energy to leave the waveguide to an external load in the other direction. Impedance matching is used at the two ends of the waveguide, and would minimize reflection from the discontinuities in dielectric properties at the axial extremeties of the system.

The electromagnetic energy flux is measured using standard electromagnetic wave detectors. The energy flux in either axial direction is measured at several axial positions. The measurement allows determination of the spatial distribution of energy deposition, and enables us to evaluate the assumptions in the heat generation rate model under single- and two-phase conditions.

Under boiling conditions, the dielectric properties of the liquid contained in the waveguide would depend on the two-phase liquid-vapor structure and composition, as well as on the dielectric properties of the liquid and vapor phases. The composition, moreover, would be spatially variable. The vapor volume fraction would vary in both the axial and lateral directions. In the axial direction the vapor volume fraction would vary from zero at the bottom of the container, to upwards of 0.5 at the upper regions of the mixture.

It is assumed that the two-phase liquid can be treated, as far as the physics of the electromagnetic wave interactions is concerned, as a homogeneous fluid with dielectric properties which are weighted averages of the pure liquid and pure vapor properties. This approach has been used in the literature (Van

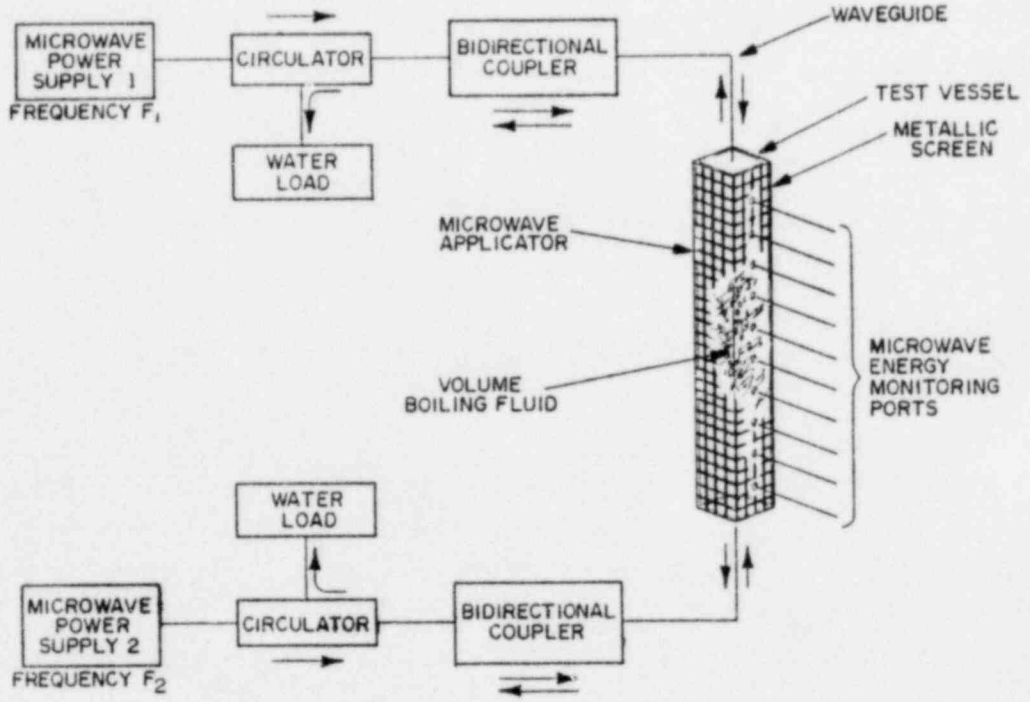

Figure 5.1 Schematic of Microwave Radiation System Proposed for Transition Phase Boiling Studies.

Beek, 1967) for two-component or two-phase applications, but needs to be verified for the vapor volume fractions likely to be encountered in the boiling systems of interest in the present work.

It is further assumed that the axial variation in dielectric properties does not lead to internal reflections within the two-phase medium. The exponential relationship for homogeneous fluids given by Equation (5.7) can be modified to account for the dielectric property variation. The attenuation coefficient, α, is now treated as a variable, and the resulting dimensionless power density (heat generation rate per unit volume of homogeneous two-phase fluid) is

$$\frac{P}{P_o} = \exp\left(-\int_o^x 2\alpha dx\right) + \exp\left(\int_\ell^x 2\alpha dx\right) \qquad (5.8)$$

The power density in the liquid phase is then given by

$$\psi_L = \frac{1}{1-\alpha}\left[\exp\left(-\int_o^x 2\alpha dx\right) + \exp\left(\int_\ell^x 2\alpha dx\right)\right] \qquad (5.9)$$

where α is a function of void fraction. The void fraction, in turn, is a function of x.

Inspection of Equation (5.9) indicates that the liquid power density in a two-phase fluid exposed to microwave radiation in a waveguide apparatus would not be uniform. The liquid power density is a nonlinear function of the liquid vapor composition. If the aforementioned assumptions are valid, then the microwave waveguide irradiation technique offers the possibility that the liquid power density can be represented analytically. If the dielectric properties of the two-phase mixture can be approximated by a weighted average of the pure liquid and pure vapor properties, then Equation (5.9) provides us with a mathematical representation for the liquid power density.

The waveguide technique for microwave irradiation of a boiling liquid can,

in principle, satisfy the objectives of the proposed transition phase boiling experimenter. Two factors lead to this conclusion:

(i) A mathematical description of the liquid power density distribution can be obtained.

(ii) Instrumentation techniques are available which can be used to provide measurements of the electromagnetic energy flux distribution. These techniques can be used to evaluate the model for the power density distribution.

The primary uncertainties in the application of the waveguide technique to the boiling simulation studies are:

(i) It must be verified that internal reflections and, hence, development of standing waves, can be effectively eliminated by impedance matching techniques.

(ii) It must be shown that the electromagnetic wave interactions with a two-phase dielectric can be approximated by assuming that the fluid is locally homogeneous, and that the dielectric properties of the mixture can be represented by a weighted average of the pure material properties.

These uncertainties must be resolved by suitable experiments in order to support the basic conceptual approach proposed here.

5.3.3 Recommendation.

It is recommended that the volume-heated boiling simulation experiments be conducted using microwave heating and a single-mode waveguide radiation environment. It is proposed that a cyclohexane-ethanol solution of 25 mol% ethanol be used as the dielectric test fluid. It is felt that a waveguide microwave applicator provides the best of available alternatives from the standpoints of prediction of the spatial distribution of power density. The cyclohexane-ethanol liquid solution is proposed in order to provide for heating of the liquid when a dispersed droplet phase exists.

A microwave power supply with a driving frequency of 900 MHz should be

used. This frequency, a standard in the industry, would provide a wavelength of approximately 300 mm and would, according to Figure 3.26, minimize the attenuation of power density across the cyclohexane-ethanol test fluid. The waveguide applicator would be designed to operate in a single mode with a cutoff wavelength equal to twice the lateral dimension of the waveguide (see Section 5.3.2). The choice of λ = 300 mm, therefore, fixes the lateral dimension of the waveguide applicator and, hence, the dimension of the test fluid container, to 150 mm.

It is recommended that, prior to specification and purchase of high-power equipment, that bench-scale tests be performed at low power (milliwatt to watt range) to work out the uncertainties discussed in Section 5.3.2. If these experiments bear out the basic concepts then a high-power (25 - 50 kw) test facility can be designed.

VI. SUMMARY AND CONCLUSIONS.

This report presents the results of a study on the feasibility of the use of microwave dielectric heating to simulate the nuclear heat source in LMFBR "transition phase" boiling simulation experiments. For the purposes of these experiments, microwave energy deposition ideally should provide a volumetrically-distributed heat source in which the energy generation rate per unit liquid volume (or liquid power density) is independent of position and liquid geometry. As a minimum requirement, the spatial distribution of heating rate should be calculable or measurable. The adequacy of microwave heating for this application is judged based upon the criterion of heating uniformity and upon the ability to approximate (analytically or experimentally) the liquid power density distribution.

A review of the literature pertinent to microwave radiation interaction with matter suggested the following:

(i) Water droplets exposed to microwave radiation would be heated in a manner which is strongly dependent on radius.

(ii) Severe spatial power density gradients are to be expected upon irradiation of centimeter-scale objects, whose dielectric properties are similar to water, with microwave radiation. Such observations are found in the literature for various geometry objects, for irradiation by plane waves in unbounded space or by irradiation in multimode cavities (microwave ovens).

(iii) Methods exist for the computation of power density distributions within homogeneous (and stratified) objects of regular geometry in unbounded space. Analytical methods for irradiation in microwave cavities have not been developed. Methods for prediction of power density distribution in heterogeneous materials exposed to microwave radiation also have not been developed.

The results of the literature review cited above pointed to the potential difficulties in the use of microwave heating as a simulator of the nuclear heat source, based upon the criteria of heating uniformity and power density distribution predictability. The present feasibility study was initiated to determine

whether combinations of liquids with suitable dielectric properties, microwave wavelength and suitable radiation enclosure could be found which would satisfy the requirements of the nuclear heating simulation outlined above.

Two aspects of liquid power density uniformity are addressed analytically. First, the effect of liquid geometry on power density is studied in order to determine whether millimeter-size droplets can be heated as efficiently as centimeter-scale liquid masses which are exposed to the same source of radiation. Both analyses and experiments were performed in this portion of the study. Second, the spatial distribution of power density across liquid slabs is studied, in order to determine whether wave interference effects, which lead to severe power density gradients, can be minimized by choice of suitable dielectric liquids. The above analyses were carried out for a variety of wavelengths within the microwave radiation band, for several dielectric liquids and for a range of temperature. Plane wave irradiation was assumed in all cases.

The studies characterized above led to the following conclusions:

(i) Water droplets in the millimeter size range absorb 1-2 orders-of-magnitude less energy per unit volume than centimeter-scale droplets exposed to the same source of radiation. The reason for this behavior is that the Rayleigh scattering regime extends only out to millimeter droplets. Laboratory experiments were performed which qualitatively support this conclusion.

(ii) Mixtures of polar and non-polar can be used to provide solutions of variable dielectric properties.

(iii) Cyclohexane-ethanol solutions extend the Rayleigh regime to centimeter radii, and provide reasonably uniform droplet power density over the range of interest. A 25 mol% ethanol solution is a suitable dielectric liquid from the standpoint of uniform droplet heating.

(iv) Standing waves are generated within slabs due to interference of transmitted waves and of internally reflected waves. These standing waves are responsible for the power density distributions computed across

the slabs. The choice of fluids does not significantly alter this conclusion.

(v) Conclusion (iv) is interpreted to imply that in a microwave cavity (oven) superposition of modes within a dielectric liquid would lead to power density gradients which cannot be predicted, for any of the dielectric liquids considered.

The above conclusions imply that a fluid (cyclohexane-ethanol) can be found which would ensure heating of a dispersed droplet regime. A microwave oven radiation environment however, provides neither heating uniformity nor the ability to predict the power density distribution. The judgement is made, therefore, that it is not appropriate to use a microwave oven for the boiling simulation studies. This conclusion, however, does not necessarily rule out the use of microwave heating, as discussed below.

The concept of using a microwave waveguide to irradiate the boiling dielectric liquid was investigated. The waveguide would be operated in a single mode, and would be driven by two sources of slightly different frequency. If impedance matching techniques can be successfully used to eliminate the internally reflected waves within the boiling dielectric liquid, and if the dielectric properties of the two-phase mixture can be represented analytically, then the power density distribution can be predicted. In addition, the microwave energy flux distribution can be measured along the axis of the waveguide.

It is concluded that the use of microwave heating, while not straightforward, is feasible for simulation of the nuclear heat source in transition phase boiling studies. A waveguide microwave radiation field, together with a cyclohexane-ethanol test fluid, together will satisfy two of the major requirements of the proposed boiling experiments: predictability of the power density distribution, and efficient heating of the liquid phase in a dispersed droplet flow regime. It is recommended that the large-scale (25 - 50 kw) test program be preceeded by a bench-scale experiment to resolve the remaining uncertainties with respect to the microwave waveguide applicator concept.

VII. ACKNOWLEDGEMENTS

The authors acknowledge with appreciation the efforts of Mr. E. Eves and Mr. R. Edgar of the Raytheon Corporation. Consultation with them on a number of occassions provided us with invaluable insights into the microwave applicator design problem. The basic idea for a single-mode microwave waveguide applicator was theirs.

We would like to acknowledge the help of Mr. Eric Schwarz and Mrs. Lauri Sweeney for their help in conducting the microwave oven experiments. We appreciate the helpful discussion with Mr. Salvadore Giordano, of the BNL Accelerator Department, on microwave waveguide fundamentals, and on methods of building microwave systems.

Finally, thanks are due to Ms. Marisa Canner for her typing skills and for her valuable help in preparation of this manuscript for publication.

VIII. REFERENCES

COLLIE, C. H., et al., "The Dielectric Properties of Water and Heavy Water," Proc. of Phys. Soc., 60, 145-160 (1948).

CRAPUCHETES, P. W., "Microwaves on the Production Line," Electronics, (March 1966).

FARAHAT, M., HENRY, R. E., and SANTORI, J., "Fuel Dispersal Experiments With Simulant Fluids," Proc. Int. Mtg. on Fast Reactor Safety and Related Physics, CONF 761001, p. 1707 (1976).

GABOR, J., et al., "Feasibility Study on the Simulation of LMFBR Meltdown Processes," ANL/RAS 75-40 (October 1975).

GINSBERG, T., JONES, O. C., Jr., and CHEN, J. C., "Flow Dynamics of Volume Heated Boiling Pools," ASME Paper No. 79-HT-102, 18th National Heat Transfer Conference, San Diego, Calif. (1979).

GREENE, G. A., JONES, O. C., Jr., ABUAF, N., and SCHWARZ, C. E., "Heat Removal Characteristics of Volume-Heated Boiling Pools With Inclined Boundaries in Bubbly Flow Regime," ASME Paper No. 79-HT-99, 18th National Heat Transfer Conference, San Diego, Calif. (1979b).

GREENE, G. A., et al., "Assessment of the Thermal Hydraulic Technology of the Transition Phase of a Core-Disruptive Accident in a LMFBR," BNL-NUREG-27366 (February 1980).

GUNN, K. L. S., and EAST, T. W. R., "The Microwave Properties of Precipitation Particles," Q. Journal of Royal Meteorological Soc., 80, 552-545 (1954).

GUY, A. W., "Electromagnetic Fields and Relative Heating Patterns Due to a Rectangular Aperture Source in Direct Contact with a Bilayered Biological Tissue," IEEE Trans. on Microwave Theory and Techniques, MTT-19, 2 (February 1971b).

GUY, A. W., et al., "Theory and Design of Microwave Heating Cavities," Bioelectromagnetic Research Librarty, U. of Washington School of Medicine, Scientific Report No. 5 (September 1975).

GUY, A. W., "Analyses of Electromagnetic Fields Induced in Biological Tissues by Thermographic Studies on Equivalent Phantom Models," IEEE Trans. on Microwave Theory and Techniques, MTT-19, 2 (February 1971a).

HO, H. S., et al., "Microwave Heating of Simulated Human Limbs by Aperture Sources," IEEE Trans. on Microwave Theory and Techniques, MTT-19, 2 (February 1971).

JAMES, C. R., et al., "Energy Conversion in Closed Microwave Cavities," Section 5.1.3 in Microwave Power Engineering, E. C. Okress, Ed., Academic Press (1968)

JOHNSON, C. C. and GUY, A. W., "Nonionizing Electromagnetic Wave Effects in Biological Materials and Systems," Proc. of the IEEE, 60, 6 (June 1972).

KERKER, M., The Scattering of Light and Other Electromagnetic Radiation, Academic Press (1969).

KOONTZ, F. A., Jr., "Volumetric Boiling: A Fundamental Study of the Phenomenon Pertaining to LMFBR Safety," M. Sc. Dissertation, Nuclear Engineering Department, Purdue University (1977).

KRAUS, J. D., Electromagnetics, McGraw-Hill (1953).

LANE, J. A. and SAXON, J. A., "Dielectric Dispersion in Pure Polar Liquids at Very High Radio Frequencies; Measurements on Water, Methyl and Ethyl Alcohols," Proc. Royal Soc. of London, 213, 400-408 (1952).

LIN, J. C., et al., "Power Deposition in a Spherical Model of a Man Exposed to 1-20 MHz Electromagnetic Fields," IEEE Trans. on Microwave Theory and Techniques, MTT-21, (December 1973).

MIE, G., Ann. Physik, 25, 377 (1908).

NYKVIST, W. E., "Microwave Meat Roasting - A computer Analysis for Cylindrical Roasts," U.S. Army Natick Research and Development Command, NATICK-TR-77/022 (July 1977).

NYKVIST, W. E. and DECAREAU, R. V., "Microwave Meat Roasting," J. Microwave Power, 11, 1 (1976).

OHLSSON, T., and BENGTSSON, N., "Microwave Heating Profiles in Foods," Microwave Energy Applied Newsletter, 4, 6 (1971).

OHLSSON, T. and RISMAN, P. O., "Temperature Distribution of Microwave Heating - Spheres and Cylinders," J. Microwave Power, 13, 4 (1978).

SAGAL, M. W. "Dielectric Relaxation in Hydrogen Bonded Liquids," Ph.D. Dissertation, Department of Chemistry, M.I.T., (August, 1961).

SCHWAN, H. P., "Radiation Biology, Medical Application, and Radiation Hazards," Section 5.2.2 in Microwave Power Engineering, E. C. Okress, Ed., Academic Press (1968).

SHAPIRO, A. R., et al., "Induced Fields and Heating Within a Cranial Structure Irradiated by an Electromagnetic Plane Wave," IEEE Trans. on Microwave Theory and Techniques, MTT-19, 2 (February 1971).

STRATTON, J. A., Electromagnetic Theory, McGraw Hill (1941).

U.S. National Bureau of Standards, "Tables of Scattering Function for Spheres," Applied Mathematics, Series 4 (January 1949).

VAN BEEK, L. K. H., "Dielectric Behavior of Heterogeneous Systems," Progress in Dielectrics, J. B. Birks, Ed. 7, Franklin Printing House, Budapest, Hungary (1967).

VAN DE HULST, H. C., Light Scattering by Small Particles, John Wiley and Sons (1957).

VON HIPPEL, A., Dielectric Materials and Application, The Technology Press of M.I.T. and John Wiley and Sons, Inc. (1954).

WATANABE, M., "Analysis of Power Density Distribution in Microwave Ovens," J. Microwave Power, 13, 2 (1978).13

WESTPHAL, W. B., Laboratory for Insulation Research, M.I.T., Private Communication (June, 1978).

APPENDIX A - GENERAL THEORY OF SCATTERING BY A SPHERE

A.1 The Wave Equation for a Sphere.

The following is a highly abbreviated summary of the scattering theory for a sphere. The reader is referred to Mie (1908), Kerker (1969) and Van de Hulst (1957) for the detailed derivations.

Maxwell's equations in general form are

$$\nabla \times \vec{E} = -\frac{\partial \vec{B}}{\partial t} \tag{A.1}$$

$$\nabla \times \vec{H} = \vec{J} + \frac{\partial \vec{D}}{\partial t} \tag{A.2}$$

$$\nabla \cdot \vec{D} = \rho \tag{A.3}$$

$$\nabla \cdot \vec{B} = 0 \tag{A.4}$$

The following material equations supplement Maxwell's equations:

$$\vec{J} = \sigma \vec{E} \tag{A.5}$$

$$\vec{D} = \varepsilon \vec{E} \tag{A.6}$$

$$\vec{B} = \mu \vec{H} \tag{A.7}$$

The electric field and magnetic field intensities, E and H satisfy the non-homogeneous equations for damped wave motion

$$\nabla^2 \vec{E} - \sigma \mu \frac{\partial \vec{E}}{\partial t} - \varepsilon \mu \frac{\partial^2 \vec{E}}{\partial x^2} = 0 \tag{A.8}$$

$$\nabla^2 \vec{H} - \sigma \mu \frac{\partial \vec{H}}{\partial t} - \varepsilon \mu \frac{\partial^2 \vec{H}}{\partial x^2} = 0 \tag{A.9}$$

It is assumed that the scalar components of E and H are represented by

$$u = u' e^{i\omega t} \tag{A.10}$$

where u' is a function of space only. Then Equations (A.8) and (A.9) reduce to the homogeneous form

$$\nabla^2 u' + k^2 u' = 0 \tag{A.11}$$

The solution to Equation (A.11) in spherical coordinates is sought, which satisfy the appropriate boundary conditions.

A.2 Solution of the Wave Equation.

The general solution of the scalar wave equation in spherical coordinates is obtained by separation of variables, and a linear superposition of all the particular solutions. The series solution is

$$r\pi(r, \theta\phi) = \sum_{n=o}^{\infty} \sum_{m=n}^{n} \left\{ c_n \psi_n(kr) + d_n X_n(kr) \right\} x \left\{ P_n^m(\cos\theta) \right\} \left\{ a_m \cos(m\phi) + b_m (\sin m\phi) \right\} \quad (A.12)$$

where the set of coefficients a_m, b_m, c_m, d_m are arbitrary constants, and π is the Hertz vector.

The constants are determined by satisfying the boundary conditions.

A.3 Scattering, Extinction and Absorption Cross Sections.

The scattering cross-section can be calculated from the expression

$$C_{SCA} = \frac{\lambda^2}{2\pi} \sum_{n=1}^{\infty} (2n+1) \left\{ |a_n|^2 + |b_n|^2 \right\} \quad (A.13)$$

and the extinction cross-section is

$$C_{EXT} = \frac{\lambda^2}{2\pi} \sum_{n=1}^{\infty} (2n+1) \left\{ \mathrm{Re}\,(a_n + b_n) \right\} \quad (A.14)$$

In terms of C_{SCAT} and C_{EXT}, the absorption cross-section is

$$C_{ABS} = C_{EXT} - C_{SCAT} \quad (A.15)$$

The scattering and absorption efficiencies are obtained from the cross-sections by normalizing with the sphere frontal area, e.g.,

$$Q_{ABS} = C_{ABS}/\pi a^2 \quad (A.16)$$

APPENDIX B - TIME-AVERAGING OF THE ELECTRIC FIELD

Consider the electromagnetic wave of the form

$$E_1 = E_{o1}\, e^{j\omega_1 t} \tag{B.1}$$

where E_{o1} is a complex quantity, independent of time, given by

$$E_{o1} = r_1 + s_1 j \tag{B.2}$$

The time-averaged, mean-square electric field intensity is given by

$$\overline{E_1^2} = \overline{\mathrm{Re}\,(E_1)\,\mathrm{Re}\,(E_1)} \tag{B.3}$$

$$= \lim_{T\to\infty} \frac{1}{T} \int_0^T \mathrm{Re}\,(E_1)\,\mathrm{Re}\,(E_1)\, dt \tag{B.4}$$

Upon integration of Equation (B.4) the result is

$$\overline{E_1^2} = \frac{1}{2}\,\mathrm{Re}\,(E_1^{*}\, E_1) \tag{B.5}$$

where the asterisk denotes "complex conjugate".

Now, consider the superposition of the two waves

$$E_1 = E_{o1}\, e^{j\omega_1 t} \tag{B.6}$$

$$E_2 = E_{02}\, e^{j\omega_2 t} \tag{B.7}$$

The net field is

$$E = E_1 + E_2 \tag{B.8}$$

The time-averaged, electric field squared is given by

$$\overline{E^2} = \overline{\mathrm{Re}\,(E)\,\mathrm{Re}\,(E)}$$

$$= \lim_{T\to\infty} \frac{1}{T} \int_0^T \mathrm{Re}\,(E)\,\mathrm{Re}(E)\, dt \tag{B.9}$$

Two cases are of interest in evaluatiion of Equation (B.9): (i) $_1 = _2$ and (ii) $\omega_1 \neq \omega_2$.

If $\omega_1 = \omega_2 = \omega$ then the field E can be written in the form

$$E = (u + vj)\, e^{j\omega t} \tag{B.10}$$

For this case the result of the integration in Equation (B.9) is identical to Equation (B.5), that is

$$\overline{E^2} = \text{Re}\,(\tilde{E}^* E) \tag{B.11}$$

For the case $\omega_1 \neq \omega_2$, such a simple form does not result. The integration, therefore, must be carried out explicitely.

APPENDIX C - TIME AVERAGE OF TWO WAVES TRAVELLING IN OPPOSITE DIRECTIONS

Consider the two plane waves

$$E_1 = E_o\, e^{j\omega_1 t}\, e^{\gamma_1^* x} \tag{C.1}$$

$$E_2 = E_o\, e^{j\omega_2 t}\, e^{-\gamma_2^* x} \tag{C.2}$$

where $\gamma_i^* = j\frac{2\pi}{\lambda} m_i^*$

$$= \frac{2\pi}{\lambda_i}\,(jn_i + n_i') \tag{C.3}$$

for $i = 1,2$. Define

$$\xi_i = \frac{2\pi}{\lambda_i} n_i \tag{C.4}$$

$$\delta_i = \frac{2\pi}{\lambda_i} n_i' \tag{C.5}$$

for $i = 1,2$.

Now compute

$$E = E_1 + E_2 \tag{C.6}$$

The field E is computed by first expressing the exponentials in Equations (C.1) and (C.2) with complex trigonometric functions. The resulting equation for E_T is given by

$$\frac{E}{E_o} = \left[\cos(\omega_1 t) + j\sin(\omega_1 t)\right]\left[\cos(\xi_1 x) + j\sin(\xi_1 x)\right] e^{\delta_1 x} + \left[\cos(\omega_2 t) + j\sin(\omega_2 t)\right]\left[\cos(\xi_2 x) - j\sin\xi_2 x\right] e^{-\delta_2 x} \tag{C.7}$$

The quantity Re (E) is then computed as

$$\frac{\mathrm{Re}\,(E)}{E_o} = \left[\cos(\omega_1 t)\cos(\xi_1 x) e^{\delta_1 x} + \cos(\omega_2 t)\cos(\xi_2 x)\, e^{-\delta_2 x}\right] - \left[\sin(\omega_1 t)\sin(\xi_1 x)\, e^{\delta_1 x} - \sin(\omega_2 t)\sin(\xi_2 x)\, e^{-\delta_2 x}\right] \tag{C.8}$$

The time-average of E^2 is computed using the relationship Equation (B.9) of Appendix B. Two cases are of interest: (i) The frequencies of the two waves are identical, i.e., $\omega_1 = \omega_2 = \omega$ and $\lambda_1 = \lambda_2 = \lambda$; (ii) The frequencies are slightly different, i.e., $\omega_1 \neq \omega_2$.

Case (i): Identical Frequencies

For this case Equation (B.11) can be applied directly. After much algebra, the result for E_T^2 is

$$\frac{\overline{E^2}}{E_o^2} = \cosh(2\delta x) + 2\cos^2(\xi x) - 1 \qquad (C.9)$$

Case (ii): Slightly Different Frequencies

For this case Equation (B.9) is applied to Equation (C.8). The result, after some algebra, is

$$\frac{\overline{E^2}}{E_o^2} = \frac{1}{2}\Big[\cos^2(\xi_1 x)\, e^{2\delta_1 x} + \cos^2(\xi_2 x)\, e^{-2\delta_2 x} + \sin^2(\xi_1 x)\, e^{2\delta_1 x} + \sin^2(\xi_2 x)\, e^{-2\delta_2 x}\Big] \qquad (C.10)$$

If the frequencies ω_1 and ω_2 are close, then

$$\delta_1 \approx \delta_2 \equiv \delta$$
$$\xi_1 \approx \xi_2 \equiv \xi$$

and Equation (C.10) reduces to

$$\frac{\overline{E^2}}{E_o^2} = \cosh(2\delta x) \qquad (C.11)$$

APPENDIX D - ELECTRIC FIELD IN A SLAB WITH BILATERAL IRRADIATION AT NORMAL INCIDENCE

Consider the slab shown in Figure 2.2, which is irradiated from both sides with sources of identical frequency and strength. The electric field within the slab denoted by Region 2, can be computed by first computing the field distribution due to single-sided irradiation. Superposition of fields can then be used to compute the fields resulting from two sources on either side of the slab. The fields in Regions 1 and 3 can be obtained similarly.

The field distribution due to the wave incident from the left side of the slab is obtained as follows: Maxwell's equations must be satisfied in each region. The field in Region 1 which satisfies Maxwell's equation is due to two waves, one travelling in the +x, the other in the -x, direction. The incident wave is reflected at the boundary 1-2. The resulting field in Region 1 is

$$E_1 = E_o\, e^{j\omega t}\, (e^{-\gamma_1^* x} + r_o\, e^{\gamma_1^* x}) \tag{D.1}$$

The field in the slab is due to two waves, one which is transmitted across boundary 1-2, and the other which is reflected back at the boundary 2-3. The resulting field in the slab (Region 2) is

$$E_2 = E_o\, t_o\, e^{j\omega t}\, (e^{-\gamma_2^* x} + r_1\, e^{\gamma_2^* x}) \tag{D.2}$$

The field in Region 3 is due simply to the wave transmitted across the 2-3 boundary, and is given by

$$E_3 = E_o\, t_o\, t_1\, e^{(j\omega t - \gamma_3^* x)} \tag{D.3}$$

The reflection coefficients (r_o and r_1) and transmission coefficients (t_o and t_1) are given by

$$r_o = \frac{Z_2 - Z_1}{Z_2 + Z_1}; \quad r_1 = \frac{Z_1 - Z_2}{Z_1 + Z_2}$$

$$t_o = \frac{2Z_2}{Z_1 + Z_2}, \quad t_1 = \frac{2Z_1}{Z_1 + Z_2} \tag{D.4}$$

A similar set of field equations is written for a wave incident from the right of the slab. The two fields are then superimposed. The resulting field

distribution within the slab due to irradiation from both sides of the slab is given as follows:

$$\frac{E_2}{E_o} = t_o e^{j\omega t} \left[e^{-\gamma_2^* x} + e^{j\omega\phi + \gamma_2^* x'} + r_1 \left(e^{\gamma_2^* x} + e^{j\omega\phi - \gamma_2^* x'} \right) \right] \tag{D.5}$$

where ϕ is the difference in phase between the two waves, and $x' = x - \ell$, where ℓ is the slab thickness.

DISTRIBUTION

BNL Department Chairman
BNL Deputy Chairman
BNL Associate Chairmen
BNL RSP Division Heads
BNL RSP Group Leaders
BNL RSE Personnel

H. Alter, DOE
L. Baker, ANL
S. G. Bankoff, Northwestern Univ.
D. Basdekas, NRC
I. Catton, Univ. of California
J. C. Chen, Lehigh Univ.
R. Coates, Sandia Laboratory
R. T. Curtis, NRC
A. Dukler, Univ. of Houston
D. T. Eggen, Northwestern Univ.
M. Epstein, ANL
J. Gabor, ANL
W. Gammill, NRC
H. H. Hummel, ANL
M. S. Kazimi, MIT
C. N. Kelber, NRC
T. Kress, ORNL
F. Kulacki, Univ. of Delaware
J. Martin, HEDL
R. Ostensen, Sandia Laboratory
A. Reynolds, Univ. of Virginia
J. Scott, LASL
M. Silberberg, NRC
R. Stein, ANL
M. Stevenson, LASL
H. Todosow, BNL
T. G. Theofanus, Purdue Univ.
J. C. Walker, Sandia Laboratory
R. W. Wright, NRC

U.S. NRC Division of Technical Information and Control